



PUBLISHED FOR SISSA BY SPRINGER

RECEIVED: March 23, 2015

REVISED: June 19, 2015

ACCEPTED: July 1, 2015

PUBLISHED: July 30, 2015

Measurement of CP asymmetries and polarisation fractions in $B_s^0 \rightarrow K^{*0} \bar{K}^{*0}$ decays



The LHCb collaboration

E-mail: paula.alvarez@cern.ch

ABSTRACT: An angular analysis of the decay $B_s^0 \rightarrow K^{*0} \bar{K}^{*0}$ is performed using pp collisions corresponding to an integrated luminosity of 1.0 fb^{-1} collected by the LHCb experiment at a centre-of-mass energy $\sqrt{s} = 7 \text{ TeV}$. A combined angular and mass analysis separates six helicity amplitudes and allows the measurement of the longitudinal polarisation fraction $f_L = 0.201 \pm 0.057 \text{ (stat.)} \pm 0.040 \text{ (syst.)}$ for the $B_s^0 \rightarrow K^*(892)^0 \bar{K}^*(892)^0$ decay. A large scalar contribution from the $K_0^*(1430)$ and $K_0^*(800)$ resonances is found, allowing the determination of additional CP asymmetries. Triple product and direct CP asymmetries are determined to be compatible with the Standard Model expectations. The branching fraction $\mathcal{B}(B_s \rightarrow K^*(892)^0 \bar{K}^*(892)^0)$ is measured to be $(10.8 \pm 2.1 \text{ (stat.)} \pm 1.4 \text{ (syst.)} \pm 0.6 (f_d/f_s)) \times 10^{-6}$.

KEYWORDS: CP violation, Hadron-Hadron Scattering, Polarization, B physics, Flavour Changing Neutral Currents

ARXIV EPRINT: [1503.05362](https://arxiv.org/abs/1503.05362)

Contents

1	Introduction	1
2	Analysis strategy	2
2.1	Angular distribution	3
2.2	Triple product asymmetries	4
2.3	Angular analysis	7
3	The LHCb detector	10
4	Event selection and signal yield	10
4.1	Acceptance properties	11
5	Triple product and direct CP asymmetries	12
6	Angular analysis	13
7	Measurement of $\mathcal{B}(B_s^0 \rightarrow K^{*0} \bar{K}^{*0})$	17
8	Conclusions	19
	The LHCb collaboration	23

1 Introduction

The $B_s^0 \rightarrow K^{*0} \bar{K}^{*0}$ decay is mediated by a $b \rightarrow s d \bar{d}$ flavour-changing neutral current (FCNC) transition, which in the Standard Model (SM) proceeds through loop diagrams at leading order. This decay has been discussed in the literature as a possible field for precision tests of the SM predictions, when it is considered in association with its U-spin symmetric channel $B^0 \rightarrow K^{*0} \bar{K}^{*0}$ [1–3]. In the SM, the expected CP violation in the former is very small, $\mathcal{O}(\lambda^2)$, with approximate cancellation between the mixing and the decay CKM phases [4]. When a scalar meson background is allowed, in addition to the vector-vector meson states, six independent helicities contribute [4].

In this paper, a search for non-SM electroweak amplitudes is reported in the decay $B_s^0 \rightarrow K^+ \pi^- K^- \pi^+$, with $K\pi$ mass close to the $K^*(892)^0$ mass, through the measurement of all CP -violating observables accessible when the flavour of the bottom-strange meson is not identified. These observables include triple products (TPs) and other CP -odd quantities [5], many of which are, as yet, experimentally unconstrained. Triple products are T -odd observables having the generic structure $\mathbf{v}_1 \cdot (\mathbf{v}_2 \times \mathbf{v}_3)$ where \mathbf{v}_i is the spin or momentum of a final-state particle. In vector-vector final states of B mesons they take the

form $\mathbf{q} \cdot (\boldsymbol{\epsilon}_1 \times \boldsymbol{\epsilon}_2)$ where \mathbf{q} is the momentum of one of the final vector mesons and $\boldsymbol{\epsilon}_1$ and $\boldsymbol{\epsilon}_2$ are their respective polarisations. Triple products are also meaningful when one of the final particles is a scalar meson.

Theoretical predictions based on perturbative QCD for the decay of B mesons into scalar-vector final states $K_0^*(1430)\bar{K}^*(892)^0$ have been recently investigated, yielding branching fractions comparable to those of vector-vector final states [6], which have been previously available [7]. The $B_s^0 \rightarrow K^{*0}\bar{K}^{*0}$ decay was first observed with 35 pb^{-1} of LHCb data [8] reporting the measurement of the branching fraction and an angular analysis. A remarkably low longitudinal polarisation fraction was observed, compatible with that found for the similar decay $B_s^0 \rightarrow \phi\phi$ [9], and at variance with that observed in the mirror channel $B^0 \rightarrow K^{*0}\bar{K}^{*0}$ [10] and with some predictions from QCD factorisation [7, 11].

An updated analysis of the $B_s^0 \rightarrow K^+\pi^-K^-\pi^+$ final state is reported in this publication, in the mass window of $\pm 150\text{ MeV}/c^2$ around the $K^*(892)^0$ (hereafter referred to as K^{*0}) mass for $K^+\pi^-$ and $K^-\pi^+$ pairs. A description of the CP observables is provided in section 2, the LHCb apparatus is summarised in section 3, and the data sample described in section 4. Triple products and direct CP asymmetries are determined in section 5. A measurement of the various amplitudes contributing to $B_s^0 \rightarrow K^+\pi^-K^-\pi^+$ is performed in section 6, under the assumption of CP conservation. These include the polarisation fractions for the vector-vector mode $B_s^0 \rightarrow K^{*0}\bar{K}^{*0}$. In light of these results, the measurement of the branching fraction $\mathcal{B}(B_s^0 \rightarrow K^{*0}\bar{K}^{*0})$ is updated in section 7. Conclusions are summarised in section 8. These studies are performed using 1.0 fb^{-1} of pp collision data from the LHC at a centre-of-mass energy of $\sqrt{s} = 7\text{ TeV}$ and recorded with the LHCb detector.

2 Analysis strategy

Considering only the S-wave ($J_{1,2} = 0$) and P-wave ($J_{1,2} = 1$) production of the $K\pi$ pairs, with $J_{1,2}$ the angular momentum of the respective $K\pi$ combination, the decay $B_s^0 \rightarrow (K^+\pi^-)_{J_1}(K^-\pi^+)_{J_2}$ can be described in terms of six helicity decay amplitudes. A two-dimensional fit to the $K^+\pi^-$ and $K^-\pi^+$ mass spectra, for masses up to the $K_J^*(1430)^0$ resonances, finds a small contribution ($< 1\%$) of tensor amplitudes when projected onto the $K\pi$ mass interval used in this analysis, and thus these amplitudes are not considered. Three of the above amplitudes describe the decay into two vector mesons, commonly referred to as P-wave amplitudes, $B_s^0 \rightarrow V_1V_2$ with $V_1 = K^{*0}$ and $V_2 = \bar{K}^{*0}$, with the subsequent two-body strong-interaction decay of each of the vector mesons into a $K\pi$ pair. Each amplitude corresponds to a different helicity ($L_z = 0, +1, -1$) of the vector mesons in the final state with respect to their relative momentum direction, H_0 , H_+ and H_- . It is useful to write the decay rate in terms of the amplitudes in the transversity basis,

$$A_0 = H_0, \quad A_{\parallel} = \frac{1}{\sqrt{2}}(H_+ + H_-) \quad \text{and} \quad A_{\perp} = \frac{1}{\sqrt{2}}(H_+ - H_-), \quad (2.1)$$

since, unlike the helicity amplitudes, they correspond to states with definite CP eigenvalues ($\eta_{\parallel} = \eta_0 = 1$ and $\eta_{\perp} = -1$). The P-wave amplitudes are assumed to have a relativistic Breit-Wigner dependence on the $K\pi$ invariant mass.

In addition, contributions arising from decays into scalar resonances or non-resonant $K\pi$ pairs need to be taken into account within the mass window indicated above. The amplitudes describing this S-wave configuration are A_{VS} , A_{SV} and A_{SS} , corresponding to the following decays¹

$$\begin{aligned} A_{VS} &: B_s^0 \rightarrow K^{*0}(K^-\pi^+)_0, \\ A_{SV} &: B_s^0 \rightarrow (K^+\pi^-)_0 \bar{K}^{*0} \quad \text{and} \\ A_{SS} &: B_s^0 \rightarrow (K^+\pi^-)_0 (K^-\pi^+)_0, \end{aligned} \quad (2.2)$$

where the subscript denotes the relative orbital angular momentum, J , of the pair. The scalar combinations $(K\pi)_0$ are described by a superposition of a broad low-mass structure related to the $K_0^*(800)$ resonance [12] and a component describing the $K_0^*(1430)$ resonance.

Unlike the $K^{*0}\bar{K}^{*0}$ final state, the S-wave configurations SV and VS defined in eq. (2.2) do not correspond to CP eigenstates. However, one may consider the following superpositions

$$\begin{aligned} |s^+\rangle &= \frac{1}{\sqrt{2}} (|K^{*0}(K^-\pi^+)_0\rangle + |(K^+\pi^-)_0 \bar{K}^{*0}\rangle) \quad \text{and} \\ |s^-\rangle &= \frac{1}{\sqrt{2}} (|K^{*0}(K^-\pi^+)_0\rangle - |(K^+\pi^-)_0 \bar{K}^{*0}\rangle), \end{aligned} \quad (2.3)$$

which are indeed CP eigenstates with opposite CP parities ($\eta_{s^+} = -1$ and $\eta_{s^-} = +1$). Therefore, it is possible to write the full decay amplitude in terms of CP -odd and CP -even amplitudes (the SS final configuration is a CP eigenstate with $\eta_{SS} = 1$) by defining

$$A_s^+ = \frac{1}{\sqrt{2}} (A_{VS} + A_{SV}) \quad \text{and} \quad A_s^- = \frac{1}{\sqrt{2}} (A_{VS} - A_{SV}). \quad (2.4)$$

2.1 Angular distribution

The angles describing the decay, $\Omega \equiv \{\theta_1, \theta_2, \varphi\}$, are shown in figure 1, where $\theta_{1(2)}$ is the angle between the direction of $K^{+(-)}$ meson and the direction opposite to the B -meson momentum in the rest frame of $V_{1(2)}$ and φ is the angle between the decay planes of the two vector mesons in the B -meson rest frame. In this angular basis, the differential decay rate describing this process is expressed as [13]

$$\begin{aligned} \frac{d^6\Gamma}{d\Omega dm_1 dm_2 dt} = N & \left| \left(\mathcal{A}_0(t) \cos\theta_1 \cos\theta_2 + \frac{\mathcal{A}_\parallel(t)}{\sqrt{2}} \sin\theta_1 \sin\theta_2 \cos\varphi \right. \right. \\ & \quad \left. \left. + i \frac{\mathcal{A}_\perp(t)}{\sqrt{2}} \sin\theta_1 \sin\theta_2 \sin\varphi \right) \mathcal{M}_1(m_1) \mathcal{M}_1(m_2) \right. \\ & \quad - \frac{\mathcal{A}_s^+(t)}{\sqrt{6}} \left(\cos\theta_1 \mathcal{M}_1(m_1) \mathcal{M}_0(m_2) - \cos\theta_2 \mathcal{M}_0(m_1) \mathcal{M}_1(m_2) \right) \\ & \quad - \frac{\mathcal{A}_s^-(t)}{\sqrt{6}} \left(\cos\theta_1 \mathcal{M}_1(m_1) \mathcal{M}_0(m_2) + \cos\theta_2 \mathcal{M}_0(m_1) \mathcal{M}_1(m_2) \right) \\ & \quad \left. - \frac{\mathcal{A}_{ss}}{3} \mathcal{M}_0(m_1) \mathcal{M}_0(m_2) \right|^2, \end{aligned} \quad (2.5)$$

¹Note that both B_s^0 and \bar{B}_s^0 can decay into these final states.

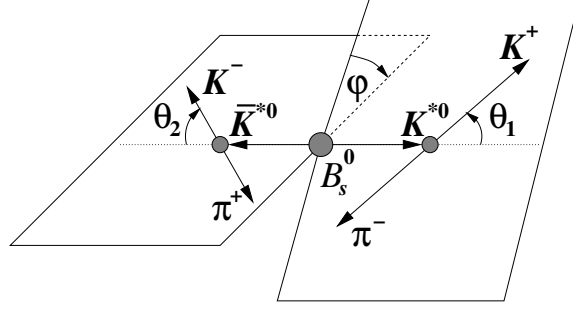


Figure 1. Definition of the angles involved in the analysis of $B_s^0 \rightarrow K^{*0} \bar{K}^{*0}$ decays.

where the different dependences of P-wave and S-wave amplitudes on the two-body masses $m_1 \equiv M(K^+\pi^-)$ and $m_2 \equiv M(K^-\pi^+)$ have been made explicit in terms of the mass propagators $\mathcal{M}_{1,0}(m)$ and N is an overall normalisation constant. The time evolution induced by $B_s^0\text{--}\bar{B}_s^0$ mixing is encoded in the time-dependence of the amplitudes $\mathcal{A}_k(t)$ ($k = 0, \parallel, \perp, s^+, s^-, ss$)

$$\mathcal{A}_k(t) = g_+(t)A_k + \left(\frac{q}{p}\right)g_-(t)\bar{A}_k, \quad (2.6)$$

where $A_k \equiv \mathcal{A}_k(t=0)$ and the time-dependent functions $g_\pm(t)$ are given by

$$g_\pm(t) = \frac{1}{2} \left(e^{-im_H t - \frac{1}{2}\Gamma_H t} \pm e^{-im_L t - \frac{1}{2}\Gamma_L t} \right) \quad (2.7)$$

with $\Gamma_{L,H}$ ($m_{L,H}$) being the width (mass) of the B_s^0 light (L) and heavy (H) mass eigenstates.

The decay rate of the CP -conjugated process, $\bar{B}_s^0 \rightarrow (K^-\pi^+)(K^+\pi^-)$, can be obtained by exchanging each amplitude A_k by $\eta_k \bar{A}_k$, where η_k is the CP eigenvalue of the final state described by A_k [4]. In this paper, due to the limited size of the available data sample, no attempt is made to identify the flavour of the initial B_s^0 meson at production, thus suppressing the sensitivity to direct and mixing-induced CP asymmetries. Nevertheless, CP violation can still be studied through the measurement of triple product asymmetries and S-wave-induced direct CP asymmetries.

2.2 Triple product asymmetries

Two TPs can be defined in B meson decays into pairs of vector particles [4, 5, 14],

$$T_1 = (\hat{n}_{V_1} \times \hat{n}_{V_2}) \cdot \hat{p}_{V_1} = \sin \varphi \quad \text{and} \quad (2.8)$$

$$T_2 = 2(\hat{n}_{V_1} \cdot \hat{n}_{V_2})(\hat{n}_{V_1} \times \hat{n}_{V_2}) \cdot \hat{p}_{V_1} = \sin 2\varphi, \quad (2.9)$$

where \hat{n}_{V_i} ($i = 1, 2$) is a unit vector perpendicular to the V_i decay plane and \hat{p}_{V_1} is a unit vector in the direction of V_1 in the B_s^0 rest frame. The observable asymmetries associated with these TPs can be calculated from integrations of the differential decay rate as [14]

$$a_T^1(t) \equiv \frac{\Gamma(\cos \theta_1 \cos \theta_2 \sin \varphi > 0, t) - \Gamma(\cos \theta_1 \cos \theta_2 \sin \varphi < 0, t)}{\Gamma(\cos \theta_1 \cos \theta_2 \sin \varphi > 0, t) + \Gamma(\cos \theta_1 \cos \theta_2 \sin \varphi < 0, t)} \quad \text{and} \quad (2.10)$$

$$a_T^2(t) \equiv \frac{\Gamma(\sin 2\varphi > 0, t) - \Gamma(\sin 2\varphi < 0, t)}{\Gamma(\sin 2\varphi > 0, t) + \Gamma(\sin 2\varphi < 0, t)}. \quad (2.11)$$

Nonzero TP asymmetries appear either due to a T -violating phase or a T -conserving phase in conjunction with final-state interactions.

When these asymmetries are measured in a sample where the production flavour is not identified, they become “true” CP -violating asymmetries, assuming that CPT is conserved. This is manifest when a_T^1 and a_T^2 are written in terms of the amplitudes defining the decay rate in eq. (2.5),

$$a_T^1 = \frac{2\sqrt{2}}{\pi} \frac{1}{\mathcal{D}} \mathcal{I}m(\mathcal{A}_\perp \mathcal{A}_0^*) \quad \text{and} \quad (2.12)$$

$$a_T^2 = -\frac{4}{\pi} \frac{1}{\mathcal{D}} \mathcal{I}m(\mathcal{A}_\perp \mathcal{A}_\parallel^*), \quad (2.13)$$

with $\mathcal{D} = |\mathcal{A}_0|^2 + |\mathcal{A}_\parallel|^2 + |\mathcal{A}_\perp|^2 + |\mathcal{A}_s^+|^2 + |\mathcal{A}_s^-|^2 + |\mathcal{A}_{ss}|^2$. Taking into account these expressions and that the decay rate contribution associated with the CP -odd amplitude \mathcal{A}_\perp changes sign under the CP transformation, the asymmetries measured in the untagged sample, A_T^i , are proportional to the CP -violating interference terms $\mathcal{I}m(\mathcal{A}_\perp \mathcal{A}_{0,\parallel}^* - \bar{\mathcal{A}}_\perp \bar{\mathcal{A}}_{0,\parallel}^*)$. Using eq. (2.6), these terms can be written as

$$\begin{aligned} \mathcal{I}m(\mathcal{A}_\perp \mathcal{A}_{0,\parallel}^* - \bar{\mathcal{A}}_\perp \bar{\mathcal{A}}_{0,\parallel}^*) = \frac{1}{2} e^{-\Gamma_s t} & \left[\mathcal{I}m(A_\perp A_{0,\parallel}^* - \bar{A}_\perp \bar{A}_{0,\parallel}^*) \cosh\left(\frac{\Delta\Gamma_s t}{2}\right) \right. \\ & \left. + \mathcal{I}m[(\bar{A}_\perp A_{0,\parallel}^* + A_\perp^* \bar{A}_{0,\parallel}) e^{-i\phi_{\text{mix}}}] \sinh\left(\frac{\Delta\Gamma_s t}{2}\right) \right], \end{aligned} \quad (2.14)$$

where $\Delta\Gamma_s \equiv \Gamma_L - \Gamma_H$, $\Gamma_s \equiv (\Gamma_L + \Gamma_H)/2$ and ϕ_{mix} is the phase in $B_s^0 - \bar{B}_s^0$ mixing. The coefficients $\mathcal{I}m(A_\perp A_{0,\parallel}^* - \bar{A}_\perp \bar{A}_{0,\parallel}^*)$ and $\mathcal{I}m[(\bar{A}_\perp A_{0,\parallel}^* + A_\perp^* \bar{A}_{0,\parallel}) e^{-i\phi_{\text{mix}}}]$ are TP and mixing-induced TP asymmetries, respectively, and are CP -violating quantities [4]. In the analysis presented in this paper, only the time-integrated asymmetries

$$A_T^1 = \frac{2\sqrt{2}}{\pi} \frac{1}{D} \int \mathcal{I}m(\mathcal{A}_\perp \mathcal{A}_0^*) dt \quad \text{and} \quad (2.15)$$

$$A_T^2 = -\frac{4}{\pi} \frac{1}{D} \int \mathcal{I}m(\mathcal{A}_\perp \mathcal{A}_\parallel^*) dt, \quad (2.16)$$

are measured ($D = \int \mathcal{D} dt$), with no identification of initial B_s^0 flavour. Thus CP -violating linear combinations of the above observables are accessible.

When the S-wave contribution is taken into account, two additional CP -even amplitudes, \mathcal{A}_s^- and \mathcal{A}_{ss} , interfere with \mathcal{A}_\perp , and give rise to two additional CP -violating terms. Further asymmetric integrations of the decay rate, analogous to those in [14], lead to the following observables

$$\begin{aligned} A_T^3 & \equiv \frac{\Gamma((\cos \theta_1 + \cos \theta_2) \sin \varphi > 0) - \Gamma((\cos \theta_1 + \cos \theta_2) \sin \varphi < 0)}{\Gamma((\cos \theta_1 + \cos \theta_2) \sin \varphi > 0) + \Gamma((\cos \theta_1 + \cos \theta_2) \sin \varphi < 0)} \\ & = \frac{32}{5\pi\sqrt{3}} \frac{1}{\mathcal{D}} \int \mathcal{I}m((\mathcal{A}_\perp \mathcal{A}_s^{-*} - \bar{\mathcal{A}}_\perp \bar{\mathcal{A}}_s^{-*}) \mathcal{M}_1(m) \mathcal{M}_0^*(m)) dm \end{aligned} \quad (2.17)$$

and

$$\begin{aligned}
 A_T^4 &\equiv \frac{\Gamma(\sin \varphi > 0) - \Gamma(\sin \varphi < 0)}{\Gamma(\sin \varphi > 0) + \Gamma(\sin \varphi < 0)} \\
 &= \frac{3\pi}{4\sqrt{2}} \frac{1}{\mathcal{D}} \int \mathcal{I}m \left((\mathcal{A}_\perp \mathcal{A}_{ss}^* - \bar{\mathcal{A}}_\perp \bar{\mathcal{A}}_{ss}^*) \mathcal{M}_1(m) \mathcal{M}_0^*(m) \right) dm,
 \end{aligned} \tag{2.18}$$

where the mass integration extends over the chosen $K\pi$ mass window. It is performed over the product of mass propagators of different resonances, times specific CP -violating observables involving \mathcal{A}_\perp .

Since \mathcal{A}_s^+ is also CP -odd, its interference terms with the CP -even amplitudes change sign under B_s^0 to \bar{B}_s^0 interchange. Consequently, four new CP -violating asymmetries are accessible from $B_s^0 \rightarrow K^+\pi^- K^-\pi^+$ decays,

$$\begin{aligned}
 A_D^1 &\equiv \frac{\Gamma(\cos \theta_1 \cos \theta_2 (\cos \theta_1 - \cos \theta_2) > 0) - \Gamma(\cos \theta_1 \cos \theta_2 (\cos \theta_1 - \cos \theta_2) < 0)}{\Gamma(\cos \theta_1 \cos \theta_2 (\cos \theta_1 - \cos \theta_2) > 0) + \Gamma(\cos \theta_1 \cos \theta_2 (\cos \theta_1 - \cos \theta_2) < 0)} \\
 &= \frac{\sqrt{2}}{5\sqrt{3}} \frac{1}{\mathcal{D}} \left[9 \int \mathcal{R}e \left((\mathcal{A}_s^+ \mathcal{A}_0^* - \bar{\mathcal{A}}_s^+ \bar{\mathcal{A}}_0^*) \mathcal{M}_0(m) \mathcal{M}_1^*(m) \right) dm \right. \\
 &\quad \left. + 5 \int \mathcal{R}e \left((\mathcal{A}_s^+ \mathcal{A}_{ss}^* - \bar{\mathcal{A}}_s^+ \bar{\mathcal{A}}_{ss}^*) \mathcal{M}_1(m) \mathcal{M}_0^*(m) \right) dm \right],
 \end{aligned} \tag{2.19}$$

$$\begin{aligned}
 A_D^2 &\equiv \frac{\Gamma((\cos \theta_1 - \cos \theta_2) \cos \varphi > 0) - \Gamma((\cos \theta_1 - \cos \theta_2) \cos \varphi < 0)}{\Gamma((\cos \theta_1 - \cos \theta_2) \cos \varphi > 0) + \Gamma((\cos \theta_1 - \cos \theta_2) \cos \varphi < 0)} \\
 &= -\frac{32}{5\pi\sqrt{3}} \frac{1}{\mathcal{D}} \int \mathcal{R}e \left((\mathcal{A}_s^+ \mathcal{A}_\parallel^* - \bar{\mathcal{A}}_s^+ \bar{\mathcal{A}}_\parallel^*) \mathcal{M}_0(m) \mathcal{M}_1^*(m) \right) dm,
 \end{aligned} \tag{2.20}$$

$$\begin{aligned}
 A_D^3 &\equiv \frac{\Gamma((\cos \theta_1 - \cos \theta_2) > 0) - \Gamma((\cos \theta_1 - \cos \theta_2) < 0)}{\Gamma((\cos \theta_1 - \cos \theta_2) > 0) + \Gamma((\cos \theta_1 - \cos \theta_2) < 0)} \\
 &= \frac{2\sqrt{2}}{5\sqrt{3}} \frac{1}{\mathcal{D}} \left[3 \int \mathcal{R}e \left((\mathcal{A}_s^+ \mathcal{A}_0^* - \bar{\mathcal{A}}_s^+ \bar{\mathcal{A}}_0^*) \mathcal{M}_0(m) \mathcal{M}_1^*(m) \right) dm \right. \\
 &\quad \left. + 5 \int \mathcal{R}e \left((\mathcal{A}_s^+ \mathcal{A}_{ss}^* - \bar{\mathcal{A}}_s^+ \bar{\mathcal{A}}_{ss}^*) \mathcal{M}_1(m) \mathcal{M}_0^*(m) \right) dm \right]
 \end{aligned} \tag{2.21}$$

and

$$\begin{aligned}
 A_D^4 &\equiv \frac{\Gamma((\cos^2 \theta_1 - \cos^2 \theta_2) > 0) - \Gamma((\cos^2 \theta_1 - \cos^2 \theta_2) < 0)}{\Gamma((\cos^2 \theta_1 - \cos^2 \theta_2) > 0) + \Gamma((\cos^2 \theta_1 - \cos^2 \theta_2) < 0)} \\
 &= \frac{1}{\mathcal{D}} \mathcal{R}e \left(\mathcal{A}_s^+ \mathcal{A}_s^{-*} - \bar{\mathcal{A}}_s^+ \bar{\mathcal{A}}_s^{-*} \right).
 \end{aligned} \tag{2.22}$$

Some of these terms have the form $\mathcal{R}e(\mathcal{A}_s^+ \mathcal{A}_k^* - \bar{\mathcal{A}}_s^+ \bar{\mathcal{A}}_k^*)$, with $k = 0, \parallel, s^-, ss$, which is characteristic of direct CP asymmetries.

As shown above, TP and several direct CP asymmetries are accessible from untagged $B_s^0 \rightarrow K^{*0} \bar{K}^{*0}$ decays, provided that a scalar $K\pi$ background component is present. These CP -violating observables are sensitive to the contributions of FCNC processes induced by neutral scalars, which are present, for example, in models with an extended Higgs sector. Constraints on possible FCNC couplings of Higgs scalars have been recently examined [15,

[16]. Non-zero values of A_T^i or A_D^i would allow the characterisation of those operators contributing to the effective Hamiltonian. In particular an enhanced contribution from $A_D^{1,2,3}$ with respect to the other observables, would reveal stronger $(V-A) \times (V+A)$ (LR) and $(V+A) \times (V-A)$ (RL) components with respect to RR and LL operators in the above models [4].

2.3 Angular analysis

Assuming that no CP violation arises in this decay, an angular analysis of the decay products determines the polarisation fractions of the $B_s^0 \rightarrow K^{*0} \bar{K}^{*0}$ decay and the contribution of the various S-wave amplitudes. The time-integrated decay rate can be expressed as

$$\frac{d^5\Gamma}{d\Omega dm_1 dm_2} = \hat{N} \sum_{n=1}^{21} K_n(m_1, m_2) F_n(\Omega), \quad (2.23)$$

where the functions K_n contain the dependence on the amplitudes entering the decay, with their corresponding mass propagators, and \hat{N} is an overall normalisation constant. The K_n functions are given in table 1 together with the decay angle functions F_n . All terms proportional to the TP and S-wave-induced CP asymmetries ($n = 5, 6, 21$ and the symmetric $A_s^+ \leftrightarrow A_s^-$ terms in $n = 8 - 11, 13 - 16$) cancel under the assumption of CP conservation.

The dependence of each amplitude on the invariant mass of the $K^+\pi^-$ and $K^-\pi^+$ pairs is given by the propagators $\mathcal{M}_J(m) \propto \mathcal{R}_J(m) \times m/q$, where q is the momentum of each meson in the rest frame of the $K\pi$ pair

$$q = \frac{\sqrt{(m^2 - (M_\pi + M_K)^2)(m^2 - (M_\pi - M_K)^2)}}{2m}. \quad (2.24)$$

The P-wave propagator, $J = 1$, is parameterised using a spin-1 relativistic Breit-Wigner resonance function

$$\mathcal{R}_1(m) = \frac{M_1 \Gamma_1(m)}{(M_1^2 - m^2) - i M_1 \Gamma_1(m)}. \quad (2.25)$$

The mass-dependent width is given by

$$\Gamma_1(m) = \Gamma_1 \frac{M_1}{m} \frac{1 + r^2 q_1^2}{1 + r^2 q^2} \left(\frac{q}{q_1} \right)^3, \quad (2.26)$$

where M_1 and Γ_1 are the $K^{*0}(892)$ resonance mass and width, r is the interaction radius and q_1 corresponds to eq. (2.24) evaluated at the resonance position (M_1).

To describe the S-wave propagator, $\mathcal{M}_0(m)$, the LASS parameterisation [17] is used, which is an effective-range elastic scattering amplitude, interfering with the $K_0^*(1430)$ resonance,

$$\mathcal{R}_0(m) \propto \frac{1}{\cot \delta_\beta - i} + e^{2i\delta_\beta} \frac{M_0 \Gamma_0(m)}{M_0^2 - m^2 - i M_0 \Gamma_0(m)}, \quad (2.27)$$

where

$$\Gamma_0(m) = \Gamma_0 \frac{M_0}{m} \left(\frac{q}{q_0} \right), \quad (2.28)$$

n	K_n	F_n
1	$\frac{1}{\Gamma_L} A_0 ^2 \mathcal{M}_1(m_1) ^2 \mathcal{M}_1(m_2) ^2$	$\cos^2 \theta_1 \cos^2 \theta_2$
2	$\frac{1}{\Gamma_L} A_{\parallel} ^2 \mathcal{M}_1(m_1) ^2 \mathcal{M}_1(m_2) ^2$	$\frac{1}{2} \sin^2 \theta_1 \sin^2 \theta_2 \cos^2 \varphi$
3	$\frac{1}{\Gamma_H} A_{\perp} ^2 \mathcal{M}_1(m_1) ^2 \mathcal{M}_1(m_2) ^2$	$\frac{1}{2} \sin^2 \theta_1 \sin^2 \theta_2 \sin^2 \varphi$
4	$\frac{1}{\Gamma_L} A_{\parallel} A_0 \cos \delta_{\parallel} \mathcal{M}_1(m_1) ^2 \mathcal{M}_1(m_2) ^2$	$\frac{1}{2\sqrt{2}} \sin 2\theta_1 \sin 2\theta_2 \cos \varphi$
5	0	$-\frac{1}{2\sqrt{2}} \sin 2\theta_1 \sin 2\theta_2 \sin \varphi$
6	0	$-\frac{1}{2} \sin^2 \theta_1 \sin^2 \theta_2 \sin 2\varphi$
7	$\frac{1}{2} \left(\frac{ A_s^+ ^2}{\Gamma_H} + \frac{ A_s^- ^2}{\Gamma_L} \right) \mathcal{M}_1(m_1) ^2 \mathcal{M}_0(m_2) ^2$	$\frac{1}{3} \cos^2 \theta_1$
8	$\frac{1}{\sqrt{2}} \frac{1}{\Gamma_L} A_s^- A_0 \text{Re}(e^{i\delta_s^-} \mathcal{M}_1^*(m_2) \mathcal{M}_0(m_2)) \mathcal{M}_1(m_1) ^2$	$-\frac{2}{\sqrt{3}} \cos^2 \theta_1 \cos \theta_2$
9	$\frac{1}{\sqrt{2}} \frac{1}{\Gamma_L} A_s^- A_{\parallel} \text{Re}(e^{i(\delta_s^- - \delta_{\parallel})} \mathcal{M}_1^*(m_2) \mathcal{M}_0(m_2)) \mathcal{M}_1(m_1) ^2$	$-\frac{1}{\sqrt{6}} \sin 2\theta_1 \sin \theta_2 \cos \varphi$
10	$\frac{1}{\sqrt{2}} \frac{1}{\Gamma_H} A_s^+ A_{\perp} \text{Im}(e^{i(\delta_{\perp} - \delta_s^+)} \mathcal{M}_0^*(m_2) \mathcal{M}_0(m_2)) \mathcal{M}_1(m_1) ^2$	$\frac{1}{\sqrt{6}} \sin 2\theta_1 \sin \theta_2 \sin \varphi$
11	$\frac{1}{\sqrt{2}} \frac{1}{\Gamma_L} A_s^- A_{ss} \text{Re}(e^{i(\delta_s^- - \delta_{ss})} \mathcal{M}_0^*(m_1) \mathcal{M}_1(m_1)) \mathcal{M}_0(m_2) ^2$	$\frac{2}{3\sqrt{3}} \cos \theta_1$
12	$\frac{1}{2} \left(\frac{ A_s^+ ^2}{\Gamma_H} + \frac{ A_s^- ^2}{\Gamma_L} \right) \mathcal{M}_0(m_1) ^2 \mathcal{M}_1(m_2) ^2$	$\frac{1}{3} \cos^2 \theta_2$
13	$-\frac{1}{\sqrt{2}} \frac{1}{\Gamma_L} A_s^- A_0 \text{Re}(e^{i\delta_s^-} \mathcal{M}_1^*(m_1) \mathcal{M}_0(m_1)) \mathcal{M}_1(m_2) ^2$	$\frac{2}{\sqrt{3}} \cos \theta_1 \cos^2 \theta_2$
14	$-\frac{1}{\sqrt{2}} \frac{1}{\Gamma_L} A_s^- A_{\parallel} \text{Re}(e^{i(\delta_s^- - \delta_{\parallel})} \mathcal{M}_1^*(m_1) \mathcal{M}_0(m_1)) \mathcal{M}_1(m_2) ^2$	$\frac{1}{\sqrt{6}} \sin \theta_1 \sin 2\theta_2 \cos \varphi$
15	$\frac{1}{\sqrt{2}} \frac{1}{\Gamma_H} A_s^+ A_{\perp} \text{Im}(e^{i(\delta_{\perp} - \delta_s^+)} \mathcal{M}_0^*(m_1) \mathcal{M}_0(m_1)) \mathcal{M}_1(m_2) ^2$	$-\frac{1}{\sqrt{6}} \sin \theta_1 \sin 2\theta_2 \sin \varphi$
16	$-\frac{1}{\sqrt{2}} \frac{1}{\Gamma_L} A_s^- A_{ss} \text{Re}(e^{i(\delta_s^- - \delta_{ss})} \mathcal{M}_0^*(m_2) \mathcal{M}_1(m_2)) \mathcal{M}_0(m_1) ^2$	$-\frac{2}{3\sqrt{3}} \cos \theta_2$
17	$\left(\frac{ A_s^+ ^2}{\Gamma_H} - \frac{ A_s^- ^2}{\Gamma_L} \right) \text{Re}(\mathcal{M}_1^*(m_1) \mathcal{M}_0^*(m_2) \mathcal{M}_0(m_1) \mathcal{M}_1(m_2))$	$-\frac{1}{3} \cos \theta_1 \cos \theta_2$
18	$\frac{1}{\Gamma_L} A_{ss} ^2 \mathcal{M}_0(m_1) ^2 \mathcal{M}_0(m_2) ^2$	$\frac{1}{9}$
19	$\frac{1}{\Gamma_L} A_{ss} A_0 \text{Re}(e^{i\delta_{ss}} \mathcal{M}_1^*(m_1) \mathcal{M}_1^*(m_2) \mathcal{M}_0(m_1) \mathcal{M}_0(m_2))$	$-\frac{2}{3} \cos \theta_1 \cos \theta_2$
20	$\frac{1}{\Gamma_L} A_{ss} A_{\parallel} \text{Re}(e^{i(\delta_{ss} - \delta_{\parallel})} \mathcal{M}_1^*(m_1) \mathcal{M}_1^*(m_2) \mathcal{M}_0(m_1) \mathcal{M}_0(m_2))$	$-\frac{\sqrt{2}}{3} \sin \theta_1 \sin \theta_2 \cos \varphi$
21	0	$\frac{\sqrt{2}}{3} \sin \theta_1 \sin \theta_2 \sin \varphi$

Table 1. Untagged time-integrated terms used in the analysis, under the assumption of no CP violation.

	$(K\pi)_0^{*0}$ $J = 0$ [17, 18]	$K^*(892)^0$ $J = 1$ [19]
M_J (MeV/ c^2)	$1435 \pm 5 \pm 5$	895.81 ± 0.19
Γ_J (MeV/ c^2)	$279 \pm 6 \pm 21$	47.4 ± 0.6
r (GeV $^{-1}$)	-	3.0 ± 0.5
a (GeV $^{-1}$)	$1.95 \pm 0.09 \pm 0.06$	-
b (GeV $^{-1}$)	$1.76 \pm 0.36 \pm 0.67$	-

Table 2. Parameters of the mass propagators used in the fit.

and the non-resonant component is described as

$$\cot \delta_\beta = \frac{1}{aq} + \frac{1}{2}bq. \quad (2.29)$$

The values of the mass propagator parameters, including the resonance masses and widths, M_J and Γ_J , and the the scattering length (a) and effective range (b), are summarized in table 2. Other shapes modelling the S-wave propagator, including an explicit Breit-Wigner contribution for the $K_0^*(800)$ resonance, are considered in the systematic uncertainties.

The normalisation of the mass propagators

$$\int |\mathcal{M}_0|^2 dm = \int |\mathcal{M}_1|^2 dm = 1 \quad (2.30)$$

in the mass range considered, together with the normalisation condition

$$|A_0|^2 + |A_\parallel|^2 + |A_\perp|^2 + |A_s^+|^2 + |A_s^-|^2 + |A_{ss}|^2 = 1, \quad (2.31)$$

guarantees the definition of the squared amplitudes as fractions of different partial waves. The polarisation fractions for the vector mode, $B_s^0 \rightarrow K^{*0} \bar{K}^{*0}$, are defined as

$$f_{L,\parallel,\perp} = \frac{|A_{0,\parallel,\perp}|^2}{|A_0|^2 + |A_\parallel|^2 + |A_\perp|^2}. \quad (2.32)$$

The overall phase of the propagators is defined such that

$$\arg[\mathcal{M}_0(M_1)] = \arg[\mathcal{M}_1(M_1)] = 0 \quad (2.33)$$

and the convention $\delta_0 \equiv \arg(A_0) = 0$ is adopted. Therefore δ_\parallel , δ_\perp , δ_s^- , δ_s^+ and δ_{ss} are defined as the phase difference between the corresponding amplitude and A_0 at the K^{*0} mass pole. As a consequence of the lack of initial B_s^0 or \bar{B}_s^0 flavour information, the phases δ_\perp and δ_s^+ can not be measured independently, and only their difference is accessible to this analysis.

3 The LHCb detector

The LHCb detector [20, 21] is a single-arm forward spectrometer covering the pseudorapidity range $2 < \eta < 5$, designed for the study of particles containing b or c quarks. The detector includes a high-precision tracking system consisting of a silicon-strip vertex detector surrounding the pp interaction region, a large-area silicon-strip detector located upstream of a dipole magnet with a bending power of about 4 Tm, and three stations of silicon-strip detectors and straw drift tubes placed downstream of the magnet. The tracking system provides a measurement of momentum, p , of charged particles with a relative uncertainty that varies from 0.5% at low momentum to 1.0% at 200 GeV/ c . The minimum distance of a track to a primary vertex, the impact parameter (IP), is measured with a resolution of $(15 + 29/p_T) \mu\text{m}$, where p_T is the component of the momentum transverse to the beam, in GeV/ c . Different types of charged hadrons are distinguished using information from two ring-imaging Cherenkov detectors. Photons, electrons and hadrons are identified by a calorimeter system consisting of scintillating-pad and preshower detectors, an electromagnetic calorimeter and a hadronic calorimeter. Muons are identified by a system composed of alternating layers of iron and multiwire proportional chambers. The online event selection is performed by a trigger, which consists of a hardware stage, based on information from the calorimeter and muon systems, followed by a software stage, which applies a full event reconstruction.

In the analysis presented here, all hardware triggers are used. The software trigger requires a multi-track secondary vertex with a significant displacement from the primary pp interaction vertices (PVs). At least one charged particle must have a transverse momentum $p_T > 1.7 \text{ GeV}/c$ and be inconsistent with originating from a PV. A multivariate algorithm [22] identifies secondary vertices consistent with the decay of a b hadron.

Simulated $B_s^0 \rightarrow K^{*0} \bar{K}^{*0}$ events are used to characterise the detector response to signal events. In the simulation, pp collisions are generated using PYTHIA [23] with a specific LHCb configuration [24]. Decays of hadronic particles are described by EVTGEN [25], in which final-state radiation is generated using PHOTOS [26]. The interaction of the generated particles with the detector and its response are implemented using the GEANT4 toolkit [27, 28] as described in ref. [29].

4 Event selection and signal yield

The event selection is similar to that used in the previous analysis [8]. K^{*0} candidates are formed from two high-quality oppositely charged tracks identified as a kaon and pion, respectively. They are selected to have $p_T > 500 \text{ MeV}/c$ and to be displaced from any PV. The $K^+ \pi^-$ and $K^- \pi^+$ pairs are required to have invariant mass within $\pm 150 \text{ MeV}/c^2$ of the known K^{*0} mass, which corresponds to 74% of the total phase-space for $B_s^0 \rightarrow K^{*0} \bar{K}^{*0}$, and $p_T > 900 \text{ MeV}/c$. Each B_s^0 candidate is constructed by combining a K^{*0} and \bar{K}^{*0} , requiring the four tracks to form a good vertex well-separated from any PV. The B_s^0 candidate invariant mass is restricted to be within the interval $[5100, 5866] \text{ MeV}/c^2$ and its momentum vector is required to point towards one PV.

In order to further discriminate the $B_s^0 \rightarrow K^{*0} \bar{K}^{*0}$ signal from the combinatorial background, different properties of the decay are combined into a multivariate discriminator [30]. The variables combined in the discriminator are the B_s^0 candidate IP with respect to the associated PV, its lifetime and p_T , the minimum χ_{IP}^2 of the four daughter tracks (defined as the difference between the χ^2 of a PV formed with and without the particle in question) with respect to the same PV and the distance of closest approach between the two K^{*0} candidates. The discriminator is trained using simulated $B_s^0 \rightarrow K^{*0} \bar{K}^{*0}$ events for signal and a small data sample excluded from the rest of the analysis as background. The optimal discriminator requirement is determined by maximising the figure of merit $N_S/\sqrt{N_S + N_B}$ in a test sample containing signal (S) and background (B) events of the same nature as those used in the training sample.

Differences in the log-likelihood for various particle identification hypotheses ($\Delta \ln \mathcal{L}_{a-b}$) are used to minimise the contamination from specific B decays. Contributions from $B^0 \rightarrow \rho \bar{K}^{*0}$ and $B^0 \rightarrow \phi K^{*0}$ modes are reduced by the $\Delta \ln \mathcal{L}_{K-\pi}$ requirements of kaons and pions. A small contamination from $\Lambda_b^0 \rightarrow p \pi^- K^- \pi^+$ decays is observed and suppressed with $\Delta \ln \mathcal{L}_{p-K}$ requirements.

An extended unbinned maximum likelihood fit to the mass spectrum of the selected $B_s^0 \rightarrow K^+ \pi^- K^- \pi^+$ candidates is performed. The signal is modelled by a sum of two Crystal Ball distributions [31] that share common mean and width. The same distribution is used to describe the B^0 decay into the same final state. Components for $B^0 \rightarrow \phi K^{*0}$ and $\Lambda_b^0 \rightarrow p \pi^- K^- \pi^+$ decays are included in the fit with shapes extracted from simulated events. The contribution from $B^0 \rightarrow \rho \bar{K}^{*0}$ decays is estimated to be negligible from simulation studies. Finally, partially reconstructed B decays are parameterised using an ARGUS distribution [32] and the remaining combinatorial background is modelled using an exponential function. The fit result is shown in figure 2. A total of 697 ± 31 $B_s^0 \rightarrow K^+ \pi^- K^- \pi^+$ decays is obtained.

4.1 Acceptance properties

Effects introduced in data due to the geometry of the detector and to the selection requirements need to be taken into account in the measurement.

The study of simulated $B_s^0 \rightarrow K^{*0} \bar{K}^{*0}$ events shows that the detection and selection efficiency is not uniform as a function of the decay angles θ_1 and θ_2 , but has no dependence, at the level of precision needed for this analysis, on φ and on the invariant mass of the two $K\pi$ pairs, m_1 and m_2 . The acceptance decreases as $\cos \theta_i$ approaches 1. This feature is mainly induced by the requirement on the minimum p_T of the daughter pions. This effect is modelled by a two-dimensional function in $\cos \theta_1$ and $\cos \theta_2$, which is extracted from simulation.

Since the trigger system uses the p_T of the charged particles, the acceptance effect is different for events where signal tracks were involved in the trigger decision (called trigger-on-signal or TOS throughout) and those where the trigger decision was made using information from the rest of the event (non-TOS). The data set is split according to these two categories and a different acceptance correction is applied to each subset.

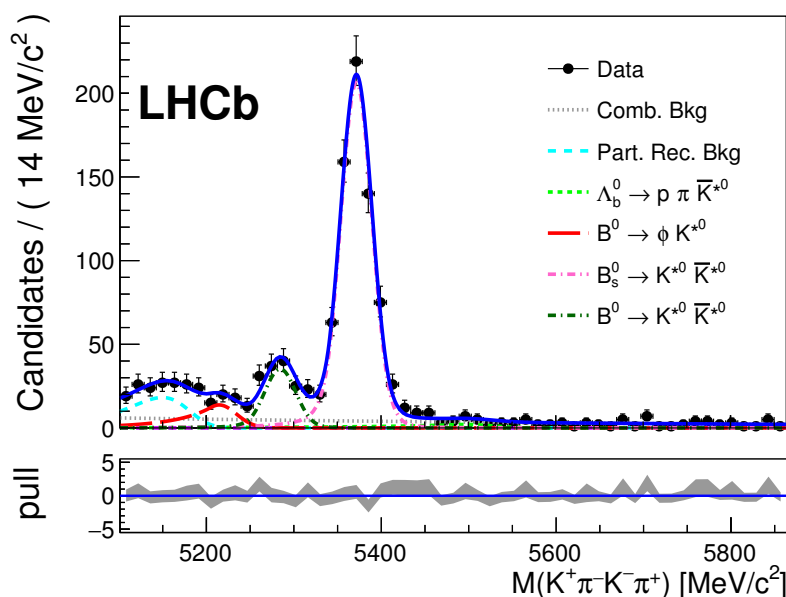


Figure 2. Invariant mass distribution for selected $K^+\pi^-K^-\pi^+$ candidates. The (blue) solid line is the result of the fit explained in the text. The B_s^0 and B^0 signal peaks are shown as as dashed-dotted lines (pink and dark green, respectively). The various peaking background components are represented as dotted lines: (red) $B^0 \rightarrow \phi K^{*0}$, (green) $\Lambda_b^0 \rightarrow p\pi^-K^-\pi^+$ and (light blue) partially reconstructed decays. The (grey) dotted line is the combinatorial background component. The normalised residual (pull) is shown below.

5 Triple product and direct CP asymmetries

Triple products and direct CP asymmetries are calculated for $B_s^0 \rightarrow K^+\pi^-K^-\pi^+$ using eqs. (2.10) and (2.11), after time integration, and eqs. (2.17)–(2.22) from those candidates with a four-body invariant mass within ± 30 MeV/ c^2 of the known B_s^0 mass. The background in this interval, which is purely combinatorial, is subtracted according to the fraction calculated from the result of the invariant mass fit, $f_{\text{bkg}} = (3.44 \pm 0.34)\%$. The angular distributions of the background are extracted from the upper mass sideband, defined by $M(K^+\pi^-K^-\pi^+) > 5550$ MeV/ c^2 . Acceptance effects are then corrected in the signal angular distributions. The measured asymmetries are listed in table 3. From the definitions given in section 2.2, correlations of the order of 5% are expected among these asymmetries, with the exception of A_D^1 and A_D^3 where the correlation is calculated to be close to 90%.

The main systematic uncertainty in these measurements is associated to the angular acceptance correction. Discrepancies in the p_T spectra and the particle identification efficiencies between data and simulation are used to modify the acceptance function obtained from simulation. Systematic uncertainties are determined from the variation in the measured asymmetries when this modified acceptance is used. Systematic effects are found to be larger in case of the four direct CP asymmetries, in particular for A_D^3 , which has

Asymmetry	Value
A_T^1	$0.003 \pm 0.041 \pm 0.009$
A_T^2	$0.009 \pm 0.041 \pm 0.009$
A_T^3	$0.019 \pm 0.041 \pm 0.008$
A_T^4	$-0.040 \pm 0.041 \pm 0.008$
A_D^1	$-0.061 \pm 0.041 \pm 0.012$
A_D^2	$0.081 \pm 0.041 \pm 0.008$
A_D^3	$-0.079 \pm 0.041 \pm 0.023$
A_D^4	$-0.081 \pm 0.041 \pm 0.010$

Table 3. Triple product and direct CP asymmetries measured in this analysis. The first uncertainties are statistical and the second systematic.

a strong dependence on $\cos \theta_{1,2}$. In addition, the lifetime-biasing selection criteria have a slightly different effect on the various amplitudes, which correspond to decays with different effective lifetimes, due to the width difference between B_s^0 mass eigenstates [33, 34]. This could induce a bias in the measured TP and direct CP asymmetries. A set of simulated experiments is performed to estimate the impact of the lifetime acceptance in the eight quantities. The observed deviations are small and are used to assign a systematic uncertainty. Finally, the effect of the uncertainty in the background contribution is estimated by changing the background fraction and the parameters in the background model within their statistical uncertainty and recalculating the asymmetries.

6 Angular analysis

The magnitudes and phases of the various amplitudes contributing to the $B_s^0 \rightarrow K^+\pi^-K^-\pi^+$ decay are determined using a five-dimensional fit to the three helicity angles (Ω) and to the invariant mass of the two $K\pi$ pairs (m_1, m_2) of all candidates with a four-body invariant mass $|M(K^+, \pi^-, K^-, \pi^+) - m_{B_s^0}| < 30 \text{ MeV}/c^2$.

The model used to describe the distribution in these five variables is given by

$$\mathcal{F}(\Omega, m_1, m_2) = (1 - f_{\text{bkg}})F(\Omega, m_1, m_2) \times \varepsilon(\Omega) + f_{\text{bkg}}F_{\text{bkg}}(\Omega, m_1, m_2), \quad (6.1)$$

where $F(\Omega, m_1, m_2)$ is the probability density function in eq. (2.5), $\varepsilon(\Omega)$ is the acceptance function modelling the effects introduced by reconstruction, selection and trigger reported in section 4.1, and $F_{\text{bkg}}(\Omega, m_1, m_2)$ describes the distribution of the background extracted from the upper mass sideband. The background fraction, f_{bkg} , is obtained from the result of the fit to the invariant mass of the B_s^0 candidates.

Using this model, an unbinned maximum likelihood fit is performed simultaneously for TOS and non-TOS $B_s^0 \rightarrow K^+\pi^-K^-\pi^+$ candidates, where only the acceptance function and the background fraction are different between the two samples. The results of the fit are summarised in table 4. Figures 3 and 4 show the angular and $K\pi$ mass projections of the

Parameter	Value
f_L	$0.201 \pm 0.057 \pm 0.040$
f_{\parallel}	$0.215 \pm 0.046 \pm 0.015$
$ A_s^+ ^2$	$0.114 \pm 0.037 \pm 0.023$
$ A_s^- ^2$	$0.485 \pm 0.051 \pm 0.019$
$ A_{ss} ^2$	$0.066 \pm 0.022 \pm 0.007$
δ_{\parallel}	$5.31 \pm 0.24 \pm 0.14$
$\delta_{\perp} - \delta_s^+$	$1.95 \pm 0.21 \pm 0.04$
δ_s^-	$1.79 \pm 0.19 \pm 0.19$
δ_{ss}	$1.06 \pm 0.27 \pm 0.23$

Table 4. Results of the simultaneous fit to $B_s^0 \rightarrow K^+\pi^-K^-\pi^+$ TOS and non-TOS candidates with $|M(K^+, \pi^-, K^-, \pi^+) - m_{B_s^0}| < 30 \text{ MeV}/c^2$ (phases are measured in radians). The first uncertainties are statistical and the second systematic.

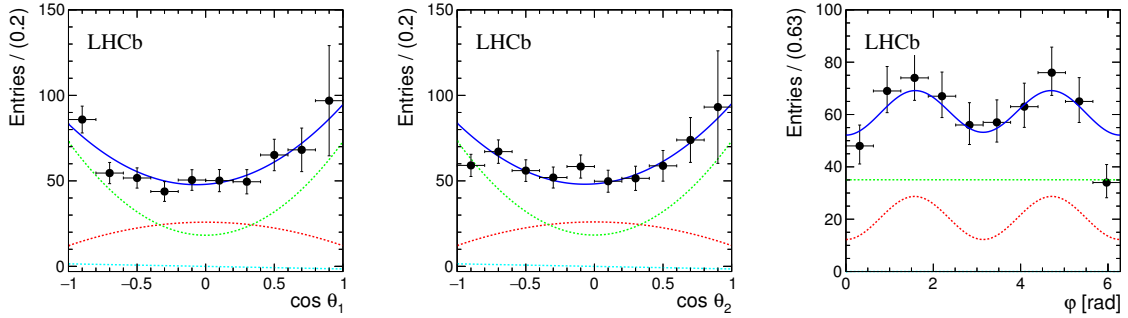


Figure 3. Results of the simultaneous fit to $B_s^0 \rightarrow K^+\pi^-K^-\pi^+$ candidates (blue solid line) in the three helicity angles. The dots represent the data after background subtraction and acceptance correction. The red dashed line is the P-wave component, the green dashed line is the S-wave component and the light-blue dashed line represents the $A_s^+ A_0$ interference term.

multi-dimensional distributions. To quantitatively demonstrate the interference between the different partial waves, a forward-backward asymmetry is defined for K^{*0} meson as $A_{\text{FB}} = (N_{\text{F}} - N_{\text{B}})/(N_{\text{F}} + N_{\text{B}})$, where N_{F} (N_{B}) is the number of K^+ mesons emitted with positive (negative) $\cos \theta_1$, and analogously for the \bar{K}^{*0} meson. Their evolution with the $K\pi$ invariant mass is shown in figure 4, as an additional projection of the fit result. According to eq. (2.5) these asymmetries are proportional to the interference term between A_s^- and A_0 .

Figure 5 shows the likelihood for the longitudinal polarisation fraction f_L , where all the other parameters are minimised at each point of the curve, depicting parabolic behaviour around the minimum. Additionally, confidence regions in the $|A_s^-|^2 - f_L$ plane are shown.

The most important systematic uncertainties in the measurement of the different amplitudes, phases and polarisation fractions are summarised in table 5. They arise mainly from uncertainties in the modelling of the $K\pi$ mass distributions and from the assumption

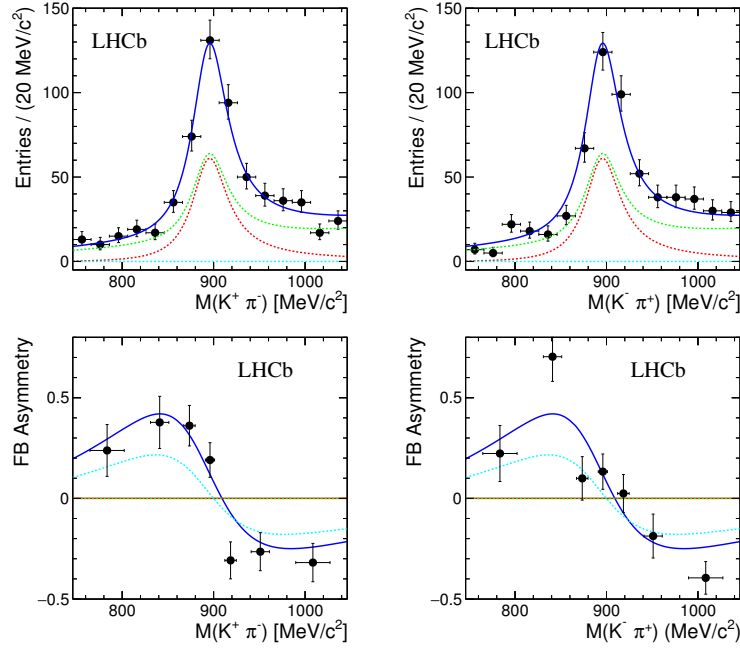


Figure 4. Projections of the model fitted to $B_s^0 \rightarrow K^+ \pi^- K^- \pi^+$ candidates (blue solid line) in the (top) invariant mass of $K\pi$ pairs and (bottom) $\cos\theta$ asymmetries as functions of $K\pi$ mass (m_1 , m_2). The dots represent the data after background subtraction and acceptance correction. The red dashed line is the P-wave component, the green dashed line is the S-wave component and the light-blue dashed line represents the $A_s^+ A_0$ interference term.

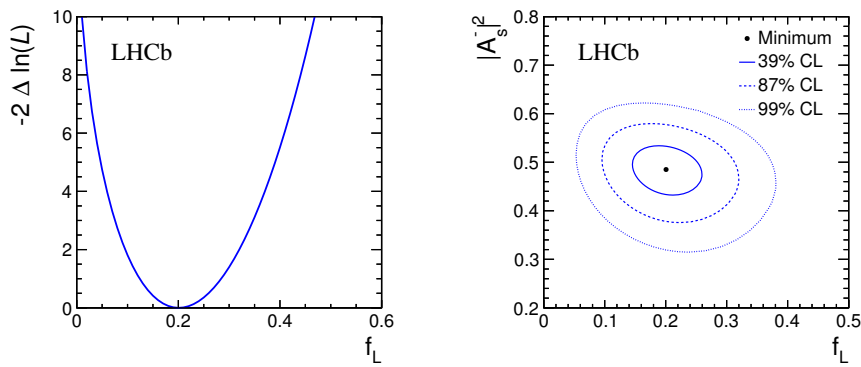


Figure 5. (Left) Profile likelihood for the parameter f_L . (Right) Regions corresponding to $\Delta \ln \mathcal{L} = 0.5, 2$ and 4.5 (39%, 87% and 99% confidence level) in the $|A_s^-|^2$ - f_L plane.

Parameter	σ_{acc}	σ_{sim}	σ_{rw}	σ_{mass}	σ_{res}	Total
f_L	0.031	0.010	0.010	0.021	0.006	0.040
f_{\parallel}	0.008	0.008	0.004	0.005	0.007	0.015
$ A_s^+ ^2$	0.019	0.005	0.002	0.011	0.003	0.023
$ A_s^- ^2$	0.007	0.007	0.010	0.003	0.012	0.019
$ A_{ss} ^2$	0.003	0.001	0.000	0.005	0.003	0.007
δ_{\parallel}	0.130	0.037	0.042	0.005	0.025	0.144
$\delta_{\perp} - \delta_s^+$	0.016	0.019	0.000	0.017	0.027	0.040
δ_s^-	0.160	0.036	0.075	0.033	0.030	0.186
δ_{ss}	0.096	0.076	0.188	0.018	0.044	0.229

Table 5. Systematic uncertainties in the measurement of the magnitude and phase of the different amplitudes contributing to the $B_s^0 \rightarrow K^+ \pi^- K^- \pi^+$ decay.

that the five-dimensional acceptance factorises into a product of two-dimensional functions. To better exploit the statistical power of the simulated sample in the less populated regions of the phase space, e.g. the tails of the mass distribution, the angular and mass acceptances are assumed to factorise. An alternative model is tested that allows for correlation between the angular distribution and the $K\pi$ invariant mass, using a two-dimensional function in $(\cos \theta_i, m_i)$, universal for K^{*0} and \bar{K}^{*0} decays. The fit is repeated with this acceptance model and a systematic uncertainty, σ_{acc} , is determined from the variation with respect to the nominal fit result. An additional uncertainty accounts for the limited size of the simulated samples, σ_{sim} .

To test the accuracy of the simulation, kinematic distributions, such as those of the p_T of final-state particles, are compared between data and simulation. Since the input amplitudes used in the generators are different from those measured in data, an iterative method is defined to disentangle the discrepancies associated with a different physical distribution. This procedure supports the quality of the simulation, and allows for the determination of the associated systematic uncertainty, σ_{rw} .

Several alternative models for the parameterisation of invariant mass propagators are used and a systematic uncertainty, σ_{mass} , for the fit parameters is estimated from the variation of the fit results. The main contribution to this uncertainty comes from the S-wave mass propagator, which is modelled by the LASS parameterisation [17] in the nominal fit. A combination of two spin-0 relativistic Breit-Wigner distributions with the mean and width of the $K_0^*(800)$ and $K_0^*(1430)$, respectively [19], and a single contribution from $K_0^*(1430)$ are also used.

Additional small uncertainties are considered to account for the effect of the invariant mass resolution, the lifetime acceptance and possible biases induced by the fitting method (σ_{res}).

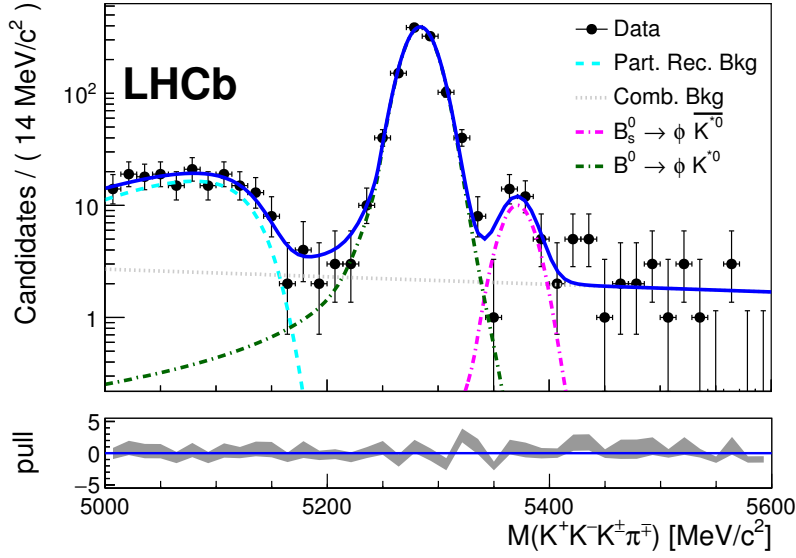


Figure 6. Invariant mass of the selected $K^+K^-K^\pm\pi^\mp$ combinations and result of the fit to the data. The points represent the data and the (blue) solid line is the fit model. The B_s^0 and B^0 signal peaks are shown as as dashed-dotted lines (pink and dark green, respectively). The contribution from partially reconstructed decays is represented as a (light blue) dashed line. The (grey) dotted line is the combinatorial background component. The normalised residual (pull) is shown below.

7 Measurement of $\mathcal{B}(B_s^0 \rightarrow K^{*0}\bar{K}^{*0})$

The branching fraction of the vector mode $B_s^0 \rightarrow K^{*0}\bar{K}^{*0}$ is updated with respect to the previous result [8]. This measurement is normalised using the $B^0 \rightarrow \phi K^{*0}$ decay, with $\phi \rightarrow K^+K^-$ and $K^{*0} \rightarrow K^+\pi^-$, which has a topology similar to the signal decay and a well-known branching fraction.

The selection of $B^0 \rightarrow \phi K^{*0}$ decays is performed such that it closely resembles the selection of $B_s^0 \rightarrow K^{*0}\bar{K}^{*0}$ decays, except for particle identification criteria. In particular, the requirements related to the B_s^0 vertex definition and the kinematic properties of the charged particles are identical. Figure 6 shows the invariant mass of the final-state particles for the selected candidates.

The ratio of branching fractions for signal and reference decay channels is given by

$$\begin{aligned} \frac{\mathcal{B}(B_s^0 \rightarrow K^{*0}\bar{K}^{*0})}{\mathcal{B}(B^0 \rightarrow \phi K^{*0})} &= \frac{\varepsilon_{B^0 \rightarrow \phi K^{*0}}^{\text{sel}}}{\varepsilon_{B_s^0 \rightarrow K^{*0}\bar{K}^{*0}}^{\text{sel}}} \times \frac{\varepsilon_{B^0 \rightarrow \phi K^{*0}}^{\text{trig}}}{\varepsilon_{B_s^0 \rightarrow K^{*0}\bar{K}^{*0}}^{\text{trig}}} \times \frac{\lambda_{f_L}(B^0 \rightarrow \phi K^{*0})}{\lambda_{f_L}(B_s^0 \rightarrow K^{*0}\bar{K}^{*0})} \\ &\times \frac{N_{B_s^0} \times f_{B_s^0 \rightarrow K^{*0}\bar{K}^{*0}}}{N_{B^0} \times f_{B^0 \rightarrow \phi K^{*0}}} \times \frac{f_d}{f_s} \times \frac{\mathcal{B}(\phi \rightarrow K^+K^-)}{\mathcal{B}(K^{*0} \rightarrow K^+\pi^-)}, \end{aligned} \quad (7.1)$$

where f_d/f_s is the ratio of probabilities for a b quark to form a B^0 or a B_s^0 meson [35, 36].

The quantities $N_{B_s^0}$ and N_{B^0} represent the number of observed candidates for $B_s^0 \rightarrow K^+\pi^-K^-\pi^+$ and $B^0 \rightarrow K^+K^-K^\pm\pi^\mp$ decays, respectively, and are determined from the

$N_{B_s^0}$	$697 \pm 31 \pm 11$
N_{B^0}	$1049 \pm 33 \pm 7$
$\kappa_{B^0 \rightarrow \phi K^{*0}} / \kappa_{B_s^0 \rightarrow K^{*0} \bar{K}^{*0}}$	$0.453 \pm 0.059 \pm 0.040$
$\varepsilon_{B^0 \rightarrow \phi K^{*0}} / \varepsilon_{B_s^0 \rightarrow K^{*0} \bar{K}^{*0}}$	$1.30 \pm 0.17 \pm 0.07$

Table 6. Summary of relevant quantities in the $\mathcal{B}(B_s^0 \rightarrow K^{*0} \bar{K}^{*0})$ calculation. The factor $\kappa(B_s^0 \rightarrow K^{*0} \bar{K}^{*0})$ is defined as $\lambda_{f_L}(B_s^0 \rightarrow K^{*0} \bar{K}^{*0})/f_{B_s^0 \rightarrow K^{*0} \bar{K}^{*0}}$, and equivalently for the $B^0 \rightarrow \phi K^{*0}$ decay. The first uncertainty is statistical, the second systematic.

corresponding fits to the four-body invariant mass spectra. The value of $N_{B_s^0}$ is reported in section 4. The yield N_{B^0} is extracted from an extended unbinned maximum likelihood fit to the spectrum in figure 6. The B^0 signal is modelled by a combination of Crystal Ball and Gaussian distributions that share a common mean. Their relative width, fraction and parameters describing the tail of the Crystal Ball function are set to the values determined from simulation. The signal from the recently observed decay $B_s^0 \rightarrow \phi \bar{K}^{*0}$ [37] is also described using this parameterisation. The mass difference between B^0 and B_s^0 mesons is fixed to the world average value [19]. The partially reconstructed background is modelled using an ARGUS distribution with parameters free to vary in the fit. The combinatorial background is parameterised with a decreasing exponential function. A total of 1049 ± 33 signal decays for the $B^0 \rightarrow K^+ K^- K^\pm \pi^\mp$ decay are observed.

The yield of candidates corresponding to the resonant decays, $B_s^0 \rightarrow K^{*0} \bar{K}^{*0}$ and $B^0 \rightarrow \phi K^{*0}$, is given by the purity factors $f_{B_s^0 \rightarrow K^{*0} \bar{K}^{*0}}$ and $f_{B^0 \rightarrow \phi K^{*0}}$. The ratio of combined reconstruction and selection efficiencies, ε^{sel} , is calculated using $B_s^0 \rightarrow K^{*0} \bar{K}^{*0}$ and $B^0 \rightarrow \phi K^{*0}$ simulated events and validated using data. The inefficiency induced by the particle identification requirements is then determined separately using large calibration samples. The ratio of trigger efficiencies, $\varepsilon^{\text{trig}}$, is computed through a data-driven method [38]. Moreover, the overall efficiency for each channel depends on the helicity angle distribution of the final state particles, and is encoded into the factors λ_{f_L} . Both the purity and λ_{f_L} factors for the $B_s^0 \rightarrow K^{*0} \bar{K}^{*0}$ decay are calculated from the results of the angular analysis. Those corresponding to $B^0 \rightarrow \phi K^{*0}$ decays are calculated from ref. [39].

With the factors summarised in table 6, the ratio of branching fractions is determined to be

$$\frac{\mathcal{B}(B_s^0 \rightarrow K^{*0} \bar{K}^{*0})}{\mathcal{B}(B^0 \rightarrow \phi K^{*0})} = 1.11 \pm 0.22(\text{stat.}) \pm 0.12(\text{syst.}) \pm 0.06(f_d/f_s). \quad (7.2)$$

Using the average $\mathcal{B}(B^0 \rightarrow \phi K^{*0}) = (9.73 \pm 0.72) \times 10^{-6}$ from the BaBar [18] and Belle [40] measurements,² corrected to take into account different rates of $B^+ B^-$ and $B^0 \bar{B}^0$ pair production from $\Upsilon(4S)$ using $\Gamma(B^+ B^-)/\Gamma(B^0 \bar{B}^0) = 1.055 \pm 0.025$ [19], the result obtained is

$$\mathcal{B}(B_s^0 \rightarrow K^{*0} \bar{K}^{*0}) = (10.8 \pm 2.1(\text{stat.}) \pm 1.4(\text{syst.}) \pm 0.6(f_d/f_s)) \times 10^{-6}.$$

²The measurement from CLEO [41] is excluded from this average since S-wave contributions were not subtracted in the determination of the branching fraction.

The main systematic uncertainties considered are related to the invariant mass fit used to determine the signal and reference event yields, the angular correction, and the determination of the trigger efficiency. To determine the systematic uncertainty associated with the number of candidates, the fit is repeated using different models for the signal and background components. The largest variation is assigned as a 1.7% systematic uncertainty. A 5% uncertainty is attributed to the trigger efficiency, after calibration of the data-driven method applied to both channels using fully simulated events. The systematic uncertainty associated with the angular correction λ_{f_L} is the result of the propagation of the systematic uncertainties evaluated for the parameters measured in the angular analysis (9%).

This result supersedes the previous measurement [8], which used a less sophisticated estimate of the S-wave contribution. If rescaled to the same S-wave fraction, both results are compatible.

As a result of $B_s^0\text{--}\bar{B}_s^0$ mixing, the time-integrated flavour-averaged branching fraction (\mathcal{B}) reported here cannot be directly compared with theoretical predictions formulated in terms of the decay amplitudes at $t = 0$ (\mathcal{B}_0). The relation between these branching fractions is given by [33]

$$\mathcal{B} = f_{\Delta\Gamma} \mathcal{B}_0, \quad \text{with} \quad f_{\Delta\Gamma} = \left(1 - \frac{\Delta\Gamma_s}{2\Gamma_s} (f_L + f_{\parallel} + f_{\perp})\right). \quad (7.3)$$

Using the decay widths measured in ref. [34] and the polarisation fractions reported here, the correction factor is calculated to be $f_{\Delta\Gamma} = 1.015 \pm 0.010$.

8 Conclusions

The decay $B_s^0 \rightarrow K^+\pi^-K^-\pi^+$ is studied using pp collision data recorded by LHCb during 2011 at a centre-of-mass energy $\sqrt{s} = 7$ TeV. This sample corresponds to an integrated luminosity of 1.0 fb^{-1} .

A test of the SM is performed by measuring eight CP -violating quantities which are predicted to be small in the SM. All of these are found to be compatible with the SM expectation, within 2σ uncertainty. In addition, assuming no CP violation, the angular distribution of the decay products is analysed as a function of the $K\pi$ pair invariant mass to measure the polarisation fractions of the decay $B_s^0 \rightarrow K^{*0}\bar{K}^{*0}$ as well as the magnitude and phase of the various S-wave amplitudes. The low polarisation of the vector-vector decay is confirmed by the measurement $f_L = 0.201 \pm 0.057$ (stat.) ± 0.040 (syst.), and a large S-wave contribution is found.

Finally, an update of the $B_s^0 \rightarrow K^{*0}\bar{K}^{*0}$ branching fraction, using the $B^0 \rightarrow \phi K^{*0}$ decay as normalisation channel, yields $\mathcal{B}(B_s^0 \rightarrow K^{*0}\bar{K}^{*0}) = (10.8 \pm 2.1 \text{ (stat.)} \pm 1.4 \text{ (syst.)} \pm 0.6 (f_d/f_s)) \times 10^{-6}$, in agreement with the theoretical prediction [7]. This result takes into account the S-wave component measured for the first time through the angular analysis of $B_s^0 \rightarrow K^+\pi^-K^-\pi^+$ decays and supersedes the measurement in ref. [8].

Acknowledgments

We express our gratitude to our colleagues in the CERN accelerator departments for the excellent performance of the LHC. We thank the technical and administrative staff at the LHCb institutes. We acknowledge support from CERN and from the national agencies: CAPES, CNPq, FAPERJ and FINEP (Brazil); NSFC (China); CNRS/IN2P3 (France); BMBF, DFG, HGF and MPG (Germany); INFN (Italy); FOM and NWO (The Netherlands); MNiSW and NCN (Poland); MEN/IFA (Romania); MinES and FANO (Russia); MinECo (Spain); SNSF and SER (Switzerland); NASU (Ukraine); STFC (United Kingdom); NSF (U.S.A.). The Tier1 computing centres are supported by IN2P3 (France), KIT and BMBF (Germany), INFN (Italy), NWO and SURF (The Netherlands), PIC (Spain), GridPP (United Kingdom). We are indebted to the communities behind the multiple open source software packages on which we depend. We are also thankful for the computing resources and the access to software R&D tools provided by Yandex LLC (Russia). Individual groups or members have received support from EPLANET, Marie Skłodowska-Curie Actions and ERC (European Union), Conseil général de Haute-Savoie, Labex ENIGMASS and OCEVU, Région Auvergne (France), RFBR (Russia), XuntaGal and GENCAT (Spain), Royal Society and Royal Commission for the Exhibition of 1851 (United Kingdom).

Open Access. This article is distributed under the terms of the Creative Commons Attribution License ([CC-BY 4.0](https://creativecommons.org/licenses/by/4.0/)), which permits any use, distribution and reproduction in any medium, provided the original author(s) and source are credited.

References

- [1] R. Fleischer, *Extracting CKM phases from angular distributions of $B_{d,s}$ decays into admixtures of CP eigenstates*, *Phys. Rev. D* **60** (1999) 073008 [[hep-ph/9903540](#)] [[INSPIRE](#)].
- [2] M. Ciuchini, M. Pierini and L. Silvestrini, *$B_s^0 \rightarrow K^{*0} \bar{K}^{*0}$ decays: the golden channels for new physics searches*, *Phys. Rev. Lett.* **100** (2008) 031802 [[hep-ph/0703137](#)] [[INSPIRE](#)].
- [3] S. Descotes-Genon, J. Matias and J. Virto, *Penguin-mediated $B_{d,s} \rightarrow VV$ decays and the B_s - \bar{B}_s mixing angle*, *Phys. Rev. D* **76** (2007) 074005 [Erratum *ibid.* **D 84** (2011) 039901] [[arXiv:0705.0477](#)] [[INSPIRE](#)].
- [4] B. Bhattacharya, A. Datta, M. Duraisamy and D. London, *Searching for new physics with $\bar{b} \rightarrow \bar{s} B_s^0 \rightarrow V_1 V_2$ penguin decays*, *Phys. Rev. D* **88** (2013) 016007 [[arXiv:1306.1911](#)] [[INSPIRE](#)].
- [5] A. Datta and D. London, *Triple-product correlations in $B \rightarrow V_1 V_2$ decays and new physics*, *Int. J. Mod. Phys. A* **19** (2004) 2505 [[hep-ph/0303159](#)] [[INSPIRE](#)].
- [6] X. Liu, Z.-J. Xiao and Z.-T. Zou, *Branching ratios and CP-violations of $B \rightarrow K_0^*(1430) K^*$ decays in the perturbative QCD approach*, *Phys. Rev. D* **88** (2013) 094003 [[arXiv:1309.7256](#)] [[INSPIRE](#)].
- [7] M. Beneke, J. Rohrer and D. Yang, *Branching fractions, polarisation and asymmetries of $B \rightarrow VV$ decays*, *Nucl. Phys. B* **774** (2007) 64 [[hep-ph/0612290](#)] [[INSPIRE](#)].
- [8] LHCb collaboration, *First observation of the decay $B_s^0 \rightarrow K^{*0} \bar{K}^{*0}$* , *Phys. Lett. B* **709** (2012) 50 [[arXiv:1111.4183](#)] [[INSPIRE](#)].

- [9] LHCb collaboration, *First measurement of the CP-violating phase in $B_s^0 \rightarrow \phi\phi$ decays*, *Phys. Rev. Lett.* **110** (2013) 241802 [[arXiv:1303.7125](#)] [[INSPIRE](#)].
- [10] BABAR collaboration, B. Aubert et al., *Observation of $B^0 \rightarrow K^{*0}\bar{K}^{*0}$ and search for $B^0 \rightarrow K^{*0}K^{*0}$* , *Phys. Rev. Lett.* **100** (2008) 081801 [[arXiv:0708.2248](#)] [[INSPIRE](#)].
- [11] S. Descotes-Genon, J. Matias and J. Virto, *An analysis of $B_{d,s}$ mixing angles in presence of new physics and an update of $B_s^0 \rightarrow K^{*0}\bar{K}^{*0}$* , *Phys. Rev. D* **85** (2012) 034010 [[arXiv:1111.4882](#)] [[INSPIRE](#)].
- [12] S. Descotes-Genon and B. Moussallam, *The $K_0^*(800)$ scalar resonance from Roy-Steiner representations of πK scattering*, *Eur. Phys. J. C* **48** (2006) 553 [[hep-ph/0607133](#)] [[INSPIRE](#)].
- [13] J.G. Korner and G.R. Goldstein, *Quark and particle helicities in hadronic charmed particle decays*, *Phys. Lett. B* **89** (1979) 105 [[INSPIRE](#)].
- [14] M. Gronau and J.L. Rosner, *Triple product asymmetries in K , $D_{(s)}$ and $B_{(s)}$ decays*, *Phys. Rev. D* **84** (2011) 096013 [[arXiv:1107.1232](#)] [[INSPIRE](#)].
- [15] G. Blankenburg, J. Ellis and G. Isidori, *Flavour-changing decays of a 125 GeV Higgs-like particle*, *Phys. Lett. B* **712** (2012) 386 [[arXiv:1202.5704](#)] [[INSPIRE](#)].
- [16] R. Harnik, J. Kopp and J. Zupan, *Flavor violating Higgs decays*, *JHEP* **03** (2013) 026 [[arXiv:1209.1397](#)] [[INSPIRE](#)].
- [17] D. Aston et al., *A study of $K^-\pi^+$ scattering in the reaction $K^-p \rightarrow K^-\pi^+n$ at 11 GeV/c*, *Nucl. Phys. B* **296** (1988) 493 [[INSPIRE](#)].
- [18] BABAR collaboration, B. Aubert et al., *Time-dependent and time-integrated angular analysis of $B \rightarrow \phi K_s^0 \pi^0$ and $B \rightarrow \phi K^\pm \pi^\mp$* , *Phys. Rev. D* **78** (2008) 092008 [[arXiv:0808.3586](#)] [[INSPIRE](#)].
- [19] PARTICLE DATA GROUP collaboration, K.A. Olive et al., *Review of particle physics*, *Chin. Phys. C* **38** (2014) 090001 [[INSPIRE](#)].
- [20] LHCb collaboration, *The LHCb detector at the LHC*, *2008 JINST* **3** S08005 [[INSPIRE](#)].
- [21] LHCb collaboration, *LHCb detector performance*, *Int. J. Mod. Phys. A* **30** (2015) 1530022 [[arXiv:1412.6352](#)] [[INSPIRE](#)].
- [22] V.V. Gligorov and M. Williams, *Efficient, reliable and fast high-level triggering using a bonsai boosted decision tree*, *2013 JINST* **8** P02013 [[arXiv:1210.6861](#)] [[INSPIRE](#)].
- [23] T. Sjöstrand, S. Mrenna and P.Z. Skands, *PYTHIA 6.4 physics and manual*, *JHEP* **05** (2006) 026 [[hep-ph/0603175](#)] [[INSPIRE](#)].
- [24] I. Belyaev et al., *Handling of the generation of primary events in Gauss, the LHCb simulation framework*, *IEEE Nucl. Sci. Symp. Conf. Rec.* (2010) 1155 [[INSPIRE](#)].
- [25] D.J. Lange, *The EvtGen particle decay simulation package*, *Nucl. Instrum. Meth. A* **462** (2001) 152 [[INSPIRE](#)].
- [26] P. Golonka and Z. Was, *PHOTOS Monte Carlo: a precision tool for QED corrections in Z and W decays*, *Eur. Phys. J. C* **45** (2006) 97 [[hep-ph/0506026](#)] [[INSPIRE](#)].
- [27] GEANT4 collaboration, J. Allison et al., *GEANT4 developments and applications*, *IEEE Trans. Nucl. Sci.* **53** (2006) 270 [[INSPIRE](#)].

- [28] GEANT4 collaboration, S. Agostinelli et al., *GEANT4: a simulation toolkit*, *Nucl. Instrum. Meth. A* **506** (2003) 250 [[INSPIRE](#)].
- [29] LHCb collaboration, *The LHCb simulation application, Gauss: design, evolution and experience*, *J. Phys. Conf. Ser.* **331** (2011) 032023 [[INSPIRE](#)].
- [30] D. Karlen, *Using projections and correlations to approximate probability distributions*, *Comput. Phys.* **12** (1998) 380 [[physics/9805018](#)] [[INSPIRE](#)].
- [31] T. Skwarnicki, *A study of the radiative cascade transitions between the Υ' and Υ resonances*, Ph.D. thesis, Institute of Nuclear Physics, Krakow Poland (1986) [DESY-F31-86-02] [[INSPIRE](#)].
- [32] ARGUS collaboration, H. Albrecht et al., *Exclusive hadronic decays of B mesons*, *Z. Phys. C* **48** (1990) 543 [[INSPIRE](#)].
- [33] K. De Bruyn, R. Fleischer, R. Kneijens, P. Koppenburg, M. Merk and N. Tuning, *Branching ratio measurements of B_s decays*, *Phys. Rev. D* **86** (2012) 014027 [[arXiv:1204.1735](#)] [[INSPIRE](#)].
- [34] LHCb collaboration, *Precision measurement of CP violation in $B_s^0 \rightarrow J/\psi K^+ K^-$ decays*, *Phys. Rev. Lett.* **114** (2015) 041801 [[arXiv:1411.3104](#)] [[INSPIRE](#)].
- [35] LHCb collaboration, *Updated average f_s/f_d b-hadron production fraction ratio for 7 TeV pp collisions*, [LHCb-CONF-2013-011](#), CERN, Geneva Switzerland (2013).
- [36] LHCb collaboration, *Determination of f_s/f_d for 7 TeV pp collisions and a measurement of the branching fraction of the decay $B^0 \rightarrow D^- K^+$* , *Phys. Rev. Lett.* **107** (2011) 211801 [[arXiv:1106.4435](#)] [[INSPIRE](#)].
- [37] LHCb collaboration, *First observation of the decay $B_s^0 \rightarrow \phi \bar{K}^{*0}$* , *JHEP* **11** (2013) 092 [[arXiv:1306.2239](#)] [[INSPIRE](#)].
- [38] R. Aaij, J. Albrecht, F. Alessio, S. Amato, E. Aslanides et al., *The LHCb trigger and its performance in 2011*, *2013 JINST* **8** P04022 [[arXiv:1211.3055](#)] [[INSPIRE](#)].
- [39] LHCb collaboration, *Measurement of polarization amplitudes and CP asymmetries in $B^0 \rightarrow \phi K^*(892)^0$* , *JHEP* **05** (2014) 069 [[arXiv:1403.2888](#)] [[INSPIRE](#)].
- [40] BELLE collaboration, M. Prim et al., *Angular analysis of $B^0 \rightarrow \phi K^*$ decays and search for CP violation at Belle*, *Phys. Rev. D* **88** (2013) 072004 [[arXiv:1308.1830](#)] [[INSPIRE](#)].
- [41] CLEO collaboration, R.A. Briere et al., *Observation of $B \rightarrow \phi K$ and $B \rightarrow \phi K^*$* , *Phys. Rev. Lett.* **86** (2001) 3718 [[hep-ex/0101032](#)] [[INSPIRE](#)].

The LHCb collaboration

R. Aaij⁴¹, B. Adeva³⁷, M. Adinolfi⁴⁶, A. Affolder⁵², Z. Ajaltouni⁵, S. Akar⁶, J. Albrecht⁹, F. Alessio³⁸, M. Alexander⁵¹, S. Ali⁴¹, G. Alkhazov³⁰, P. Alvarez Cartelle⁵³, A.A. Alves Jr^{25,38}, S. Amato², S. Amerio²², Y. Amhis⁷, L. An³, L. Anderlini^{17,g}, J. Anderson⁴⁰, R. Andreassen⁵⁷, M. Andreotti^{16,f}, J.E. Andrews⁵⁸, R.B. Appleby⁵⁴, O. Aquines Gutierrez¹⁰, F. Archilli³⁸, A. Artamonov³⁵, M. Artuso⁵⁹, E. Aslanides⁶, G. Auriemma^{25,n}, M. Baalouch⁵, S. Bachmann¹¹, J.J. Back⁴⁸, A. Badalov³⁶, C. Baesso⁶⁰, W. Baldini¹⁶, R.J. Barlow⁵⁴, C. Barschel³⁸, S. Barsuk⁷, W. Barter³⁸, V. Batozskaya²⁸, V. Battista³⁹, A. Bay³⁹, L. Beaucourt⁴, J. Beddow⁵¹, F. Bedeschi²³, I. Bediaga¹, L.J. Bel⁴¹, S. Belogurov³¹, I. Belyaev³¹, E. Ben-Haim⁸, G. Bencivenni¹⁸, S. Benson³⁸, J. Benton⁴⁶, A. Berezhnoy³², R. Bernet⁴⁰, A. Bertolin²², M.-O. Bettler⁴⁷, M. van Beuzekom⁴¹, A. Bien¹¹, S. Bifani⁴⁵, T. Bird⁵⁴, A. Bizzeti^{17,i}, T. Blake⁴⁸, F. Blanc³⁹, J. Blouw¹⁰, S. Blusk⁵⁹, V. Bocci²⁵, A. Bondar³⁴, N. Bondar^{30,38}, W. Bonivento¹⁵, S. Borghi⁵⁴, A. Borgia⁵⁹, M. Borsato⁷, T.J.V. Bowcock⁵², E. Bowen⁴⁰, C. Bozzi¹⁶, D. Brett⁵⁴, M. Britsch¹⁰, T. Britton⁵⁹, J. Brodzicka⁵⁴, N.H. Brook⁴⁶, A. Bursche⁴⁰, J. Buytaert³⁸, S. Cadeddu¹⁵, R. Calabrese^{16,f}, M. Calvi^{20,k}, M. Calvo Gomez^{36,p}, P. Campana¹⁸, D. Campora Perez³⁸, L. Capriotti⁵⁴, A. Carbone^{14,d}, G. Carboni^{24,l}, R. Cardinale^{19,38,j}, A. Cardini¹⁵, P. Carniti²⁰, L. Carson⁵⁰, K. Carvalho Akiba^{2,38}, R. Casanova Mohr³⁶, G. Casse⁵², L. Cassina^{20,k}, L. Castillo Garcia³⁸, M. Cattaneo³⁸, Ch. Cauet⁹, G. Cavallero¹⁹, R. Cenci^{23,t}, M. Charles⁸, Ph. Charpentier³⁸, M. Chefdeville⁴, S. Chen⁵⁴, S.-F. Cheung⁵⁵, N. Chiapolini⁴⁰, M. Chrzasczcz^{40,26}, X. Cid Vidal³⁸, G. Ciezarek⁴¹, P.E.L. Clarke⁵⁰, M. Clemencic³⁸, H.V. Cliff⁴⁷, J. Closier³⁸, V. Coco³⁸, J. Cogan⁶, E. Cogneras⁵, V. Cogoni^{15,e}, L. Cojocariu²⁹, G. Collazuol²², P. Collins³⁸, A. Comerma-Montells¹¹, A. Contu^{15,38}, A. Cook⁴⁶, M. Coombes⁴⁶, S. Coquereau⁸, G. Corti³⁸, M. Corvo^{16,f}, I. Counts⁵⁶, B. Couturier³⁸, G.A. Cowan⁵⁰, D.C. Craik⁴⁸, A.C. Crocombe⁴⁸, M. Cruz Torres⁶⁰, S. Cunliffe⁵³, R. Currie⁵³, C. D'Ambrosio³⁸, J. Dalseno⁴⁶, P. David⁸, P.N.Y. David⁴¹, A. Davis⁵⁷, K. De Bruyn⁴¹, S. De Capua⁵⁴, M. De Cian¹¹, J.M. De Miranda¹, L. De Paula², W. De Silva⁵⁷, P. De Simone¹⁸, C.-T. Dean⁵¹, D. Decamp⁴, M. Deckenhoff⁹, L. Del Buono⁸, N. Deléage⁴, D. Derkach⁵⁵, O. Deschamps⁵, F. Dettori³⁸, B. Dey⁴⁰, A. Di Canto³⁸, F. Di Ruscio²⁴, H. Dijkstra³⁸, S. Donleavy⁵², F. Dordei¹¹, M. Dorigo³⁹, A. Dosil Suárez³⁷, D. Dossett⁴⁸, A. Dovbnya⁴³, K. Dreimanis⁵², G. Dujany⁵⁴, F. Dupertuis³⁹, P. Durante⁶, R. Dzhelyadin³⁵, A. Dziurda²⁶, A. Dzyuba³⁰, S. Easo^{49,38}, U. Egede⁵³, V. Egorychev³¹, S. Eidelman³⁴, S. Eisenhardt⁵⁰, U. Eitschberger⁹, R. Ekelhof⁹, L. Eklund⁵¹, I. El Rifai⁵, Ch. Elsasser⁴⁰, S. Ely⁵⁹, S. Esen¹¹, H.M. Evans⁴⁷, T. Evans⁵⁵, A. Falabella¹⁴, C. Färber¹¹, C. Farinelli⁴¹, N. Farley⁴⁵, S. Farry⁵², R. Fay⁵², D. Ferguson⁵⁰, V. Fernandez Albor³⁷, F. Ferreira Rodrigues¹, M. Ferro-Luzzi³⁸, S. Filippov³³, M. Fiore^{16,f}, M. Fiorini^{16,f}, M. Firlej²⁷, C. Fitzpatrick³⁹, T. Fiutowski²⁷, P. Fol⁵³, M. Fontana¹⁰, F. Fontanelli^{19,j}, R. Forty³⁸, O. Francisco², M. Frank³⁸, C. Frei³⁸, M. Frosini¹⁷, J. Fu^{21,38}, E. Furfaro^{24,l}, A. Gallas Torreira³⁷, D. Galli^{14,d}, S. Gallorini^{22,38}, S. Gambetta^{19,j}, M. Gandelman², P. Gandini⁵⁹, Y. Gao³, J. García Pardiñas³⁷, J. Garofoli⁵⁹, J. Garra Tico⁴⁷, L. Garrido³⁶, D. Gascon³⁶, C. Gaspar³⁸, U. Gastaldi¹⁶, R. Gauld⁵⁵, L. Gavardi⁹, G. Gazzoni⁵, A. Geraci^{21,v}, E. Gersabeck¹¹, M. Gersabeck⁵⁴, T. Gershon⁴⁸, Ph. Ghez⁴, A. Gianelle²², S. Giani³⁹, V. Gibson⁴⁷, L. Giubega²⁹, V.V. Gligorov³⁸, C. Göbel⁶⁰, D. Golubkov³¹, A. Golutvin^{53,31,38}, A. Gomes^{1,a}, C. Gotti^{20,k}, M. Grabalosa Gándara⁵, R. Graciani Diaz³⁶, L.A. Granado Cardoso³⁸, E. Graugés³⁶, E. Graverini⁴⁰, G. Graziani¹⁷, A. Grecu²⁹, E. Greening⁵⁵, S. Gregson⁴⁷, P. Griffith⁴⁵, L. Grillo¹¹, O. Grünberg⁶³, B. Gui⁵⁹, E. Gushchin³³, Yu. Guz^{35,38}, T. Gys³⁸, C. Hadjivasiliou⁵⁹, G. Haefeli³⁹, C. Haen³⁸, S.C. Haines⁴⁷, S. Hall⁵³, B. Hamilton⁵⁸, T. Hampson⁴⁶, X. Han¹¹, S. Hansmann-Menzemer¹¹, N. Harnew⁵⁵, S.T. Harnew⁴⁶, J. Harrison⁵⁴, J. He³⁸, T. Head³⁹, V. Heijne⁴¹, K. Hennessy⁵², P. Henrard⁵, L. Henry⁸, J.A. Hernando Morata³⁷,

E. van Herwijnen³⁸, M. Heß⁶³, A. Hicheur², D. Hill⁵⁵, M. Hoballah⁵, C. Hombach⁵⁴, W. Hulsbergen⁴¹, T. Humair⁵³, N. Hussain⁵⁵, D. Hutchcroft⁵², D. Hynds⁵¹, M. Idzik²⁷, P. Ilten⁵⁶, R. Jacobsson³⁸, A. Jaeger¹¹, J. Jalocha⁵⁵, E. Jans⁴¹, A. Jawahery⁵⁸, F. Jing³, M. John⁵⁵, D. Johnson³⁸, C.R. Jones⁴⁷, C. Joram³⁸, B. Jost³⁸, N. Jurik⁵⁹, S. Kandybei⁴³, W. Kanso⁶, M. Karacson³⁸, T.M. Karbach³⁸, S. Karodia⁵¹, M. Kelsey⁵⁹, I.R. Kenyon⁴⁵, M. Kenzie³⁸, T. Ketel⁴², B. Khanji^{20,38,k}, C. Khurewathanakul³⁹, S. Klaver⁵⁴, K. Klimaszewski²⁸, O. Kochebina⁷, M. Kolpin¹¹, I. Komarov³⁹, R.F. Koopman⁴², P. Koppenburg^{41,38}, M. Korolev³², L. Kravchuk³³, K. Kreplin¹¹, M. Kreps⁴⁸, G. Krocker¹¹, P. Krokovny³⁴, F. Kruse⁹, W. Kucewicz^{26,o}, M. Kucharczyk^{20,k}, V. Kudryavtsev³⁴, K. Kurek²⁸, T. Kvaratskheliya³¹, V.N. La Thi³⁹, D. Lacarrere³⁸, G. Lafferty⁵⁴, A. Lai¹⁵, D. Lambert⁵⁰, R.W. Lambert⁴², G. Lanfranchi¹⁸, C. Langenbruch⁴⁸, B. Langhans³⁸, T. Latham⁴⁸, C. Lazzeroni⁴⁵, R. Le Gac⁶, J. van Leerdam⁴¹, J.-P. Lees⁴, R. Lefèvre⁵, A. Leflat³², J. Lefrançois⁷, O. Leroy⁶, T. Lesiak²⁶, B. Leverington¹¹, Y. Li⁷, T. Likhomanenko⁶⁴, M. Liles⁵², R. Lindner³⁸, C. Linn³⁸, F. Lionetto⁴⁰, B. Liu¹⁵, S. Lohn³⁸, I. Longstaff⁵¹, J.H. Lopes², P. Lowdon⁴⁰, D. Lucchesi^{22,r}, H. Luo⁵⁰, A. Lupato²², E. Luppi^{16,f}, O. Lupton⁵⁵, F. Machefert⁷, I.V. Machikhiliyan³¹, F. Maciuc²⁹, O. Maev³⁰, S. Malde⁵⁵, A. Malinin⁶⁴, G. Manca^{15,e}, G. Mancinelli⁶, P. Manning⁵⁹, A. Mapelli³⁸, J. Maratas⁵, J.F. Marchand⁴, U. Marconi¹⁴, C. Marin Benito³⁶, P. Marino^{23,t}, R. Märki³⁹, J. Marks¹¹, G. Martellotti²⁵, M. Martinelli³⁹, D. Martinez Santos⁴², F. Martinez Vidal⁶⁶, D. Martins Tostes², A. Massafferri¹, R. Matev³⁸, Z. Mathe³⁸, C. Matteuzzi²⁰, A. Mauri⁴⁰, B. Maurin³⁹, A. Mazurov⁴⁵, M. McCann⁵³, J. McCarthy⁴⁵, A. McNab⁵⁴, R. McNulty¹², B. McSkelly⁵², B. Meadows⁵⁷, F. Meier⁹, M. Meissner¹¹, M. Merk⁴¹, D.A. Milanese⁶², M.-N. Minard⁴, J. Molina Rodriguez⁶⁰, S. Monteil⁵, M. Morandin²², P. Morawski²⁷, A. Mordà⁶, M.J. Morello^{23,t}, J. Moron²⁷, A.-B. Morris⁵⁰, R. Mountain⁵⁹, F. Muheim⁵⁰, K. Müller⁴⁰, M. Mussini¹⁴, B. Muster³⁹, P. Naik⁴⁶, T. Nakada³⁹, R. Nandakumar⁴⁹, I. Nasteva², M. Needham⁵⁰, N. Neri²¹, S. Neubert¹¹, N. Neufeld³⁸, M. Neuner¹¹, A.D. Nguyen³⁹, T.D. Nguyen³⁹, C. Nguyen-Mau^{39,q}, M. Nicol⁷, V. Niess⁵, R. Niet⁹, N. Nikitin³², T. Nikodem¹¹, A. Novoselov³⁵, D.P. O'Hanlon⁴⁸, A. Oblakowska-Mucha²⁷, V. Obraztsov³⁵, S. Ogilvy⁵¹, O. Okhrimenko⁴⁴, R. Oldeman^{15,e}, C.J.G. Onderwater⁶⁷, B. Osorio Rodrigues¹, J.M. Otalora Goicochea², A. Otto³⁸, P. Owen⁵³, A. Oyanguren⁶⁶, B.K. Pal⁵⁹, A. Palano^{13,c}, F. Palombo^{21,u}, M. Palutan¹⁸, J. Panman³⁸, A. Papanestis⁴⁹, M. Pappagallo⁵¹, L.L. Pappalardo^{16,f}, C. Parkes⁵⁴, C.J. Parkinson^{9,45}, G. Passaleva¹⁷, G.D. Patel⁵², M. Patel⁵³, C. Patrignani^{19,j}, A. Pearce^{54,49}, A. Pellegrino⁴¹, G. Penso^{25,m}, M. Pepe Altarelli³⁸, S. Perazzini^{14,d}, P. Perret⁵, L. Pescatore⁴⁵, K. Petridis⁴⁶, A. Petrolini^{19,j}, E. Picatoste Olloqui³⁶, B. Pietrzyk⁴, T. Pilar⁴⁸, D. Pinci²⁵, A. Pistone¹⁹, S. Playfer⁵⁰, M. Plo Casasus³⁷, F. Polci⁸, A. Poluektov^{48,34}, I. Polyakov³¹, E. Polcarpo², A. Popov³⁵, D. Popov¹⁰, B. Popovici²⁹, C. Potterat², E. Price⁴⁶, J.D. Price⁵², J. Prisciandaro³⁹, A. Pritchard⁵², C. Prouve⁴⁶, V. Pugatch⁴⁴, A. Puig Navarro³⁹, G. Punzi^{23,s}, W. Qian⁴, R. Quagliani^{7,46}, B. Rachwal²⁶, J.H. Rademacker⁴⁶, B. Rakotomiamanana³⁹, M. Rama²³, M.S. Rangel², I. Raniuk⁴³, N. Rauschmayr³⁸, G. Raven⁴², F. Redi⁵³, S. Reichert⁵⁴, M.M. Reid⁴⁸, A.C. dos Reis¹, S. Ricciardi⁴⁹, S. Richards⁴⁶, M. Rihl³⁸, K. Rinnert⁵², V. Rives Molina³⁶, P. Robbe⁷, A.B. Rodrigues¹, E. Rodrigues⁵⁴, P. Rodriguez Perez⁵⁴, S. Roiser³⁸, V. Romanovsky³⁵, A. Romero Vidal³⁷, M. Rotondo²², J. Rouvinet³⁹, T. Ruf³⁸, H. Ruiz³⁶, P. Ruiz Valls⁶⁶, J.J. Saborido Silva³⁷, N. Sagidova³⁰, P. Sail⁵¹, B. Saitta^{15,e}, V. Salustino Guimaraes², C. Sanchez Mayordomo⁶⁶, B. Sanmartin Sedes³⁷, R. Santacesaria²⁵, C. Santamarina Rios³⁷, E. Santovetti^{24,l}, A. Sarti^{18,m}, C. Satriano^{25,n}, A. Satta²⁴, D.M. Saunders⁴⁶, D. Savrina^{31,32}, M. Schiller³⁸, H. Schindler³⁸, M. Schlupp⁹, M. Schmelling¹⁰, B. Schmidt³⁸, O. Schneider³⁹, A. Schopper³⁸, M.-H. Schune⁷, R. Schwemmer³⁸, B. Sciascia¹⁸, A. Sciubba^{25,m}, A. Semennikov³¹, I. Sepp⁵³, N. Serra⁴⁰, J. Serrano⁶, L. Sestini²², P. Seyfert¹¹, M. Shapkin³⁵, I. Shapoval^{16,43,f},

Y. Shcheglov³⁰, T. Shears⁵², L. Shekhtman³⁴, V. Shevchenko⁶⁴, A. Shires⁹, R. Silva Coutinho⁴⁸, G. Simi²², M. Sirendi⁴⁷, N. Skidmore⁴⁶, I. Skillicorn⁵¹, T. Skwarnicki⁵⁹, N.A. Smith⁵², E. Smith^{55,49}, E. Smith⁵³, J. Smith⁴⁷, M. Smith⁵⁴, H. Snoek⁴¹, M.D. Sokoloff⁵⁷, F.J.P. Soler⁵¹, F. Soomro³⁹, D. Souza⁴⁶, B. Souza De Paula², B. Spaan⁹, P. Spradlin⁵¹, S. Sridharan³⁸, F. Stagni³⁸, M. Stahl¹¹, S. Stahl³⁸, O. Steinkamp⁴⁰, O. Stenyakin³⁵, F. Sterpka⁵⁹, S. Stevenson⁵⁵, S. Stoica²⁹, S. Stone⁵⁹, B. Storaci⁴⁰, S. Stracka^{23,t}, M. Straticiuc²⁹, U. Straumann⁴⁰, R. Stroili²², L. Sun⁵⁷, W. Sutcliffe⁵³, K. Swientek²⁷, S. Swientek⁹, V. Syropoulos⁴², M. Szczekowski²⁸, P. Szczypka^{39,38}, T. Szumlak²⁷, S. T’Jampens⁴, M. Teklishyn⁷, G. Tellarini^{16,f}, F. Teubert³⁸, C. Thomas⁵⁵, E. Thomas³⁸, J. van Tilburg⁴¹, V. Tisserand⁴, M. Tobin³⁹, J. Todd⁵⁷, S. Tol⁴², L. Tomassetti^{16,f}, D. Tonelli³⁸, S. Topp-Joergensen⁵⁵, N. Torr⁵⁵, E. Tournefier⁴, S. Tourneur³⁹, K. Trabelsi³⁹, M.T. Tran³⁹, M. Tresch⁴⁰, A. Trisovic³⁸, A. Tsaregorodtsev⁶, P. Tsopelas⁴¹, N. Tuning^{41,38}, M. Ubeda Garcia³⁸, A. Ukleja²⁸, A. Ustyuzhanin⁶⁵, U. Uwer¹¹, C. Vacca^{15,e}, V. Vagnoni¹⁴, G. Valenti¹⁴, A. Vallier⁷, R. Vazquez Gomez¹⁸, P. Vazquez Regueiro³⁷, C. Vázquez Sierra³⁷, S. Vecchi¹⁶, J.J. Velthuis⁴⁶, M. Veltri^{17,h}, G. Veneziano³⁹, M. Vesterinen¹¹, J.V. Viana Barbosa³⁸, B. Viaud⁷, D. Vieira², M. Vieites Diaz³⁷, X. Vilasis-Cardona^{36,p}, A. Vollhardt⁴⁰, D. Volyanskyy¹⁰, D. Voong⁴⁶, A. Vorobyev³⁰, V. Vorobyev³⁴, C. Voß⁶³, J.A. de Vries⁴¹, R. Waldi⁶³, C. Wallace⁴⁸, R. Wallace¹², J. Walsh²³, S. Wandernoth¹¹, J. Wang⁵⁹, D.R. Ward⁴⁷, N.K. Watson⁴⁵, D. Websdale⁵³, M. Whitehead⁴⁸, D. Wiedner¹¹, G. Wilkinson^{55,38}, M. Wilkinson⁵⁹, M.P. Williams⁴⁵, M. Williams⁵⁶, H.W. Wilschut⁶⁷, F.F. Wilson⁴⁹, J. Wimberley⁵⁸, J. Wishahi⁹, W. Wislicki²⁸, M. Witek²⁶, G. Wormser⁷, S.A. Wotton⁴⁷, S. Wright⁴⁷, K. Wyllie³⁸, Y. Xie⁶¹, Z. Xing⁵⁹, Z. Xu³⁹, Z. Yang³, X. Yuan³⁴, O. Yushchenko³⁵, M. Zangoli¹⁴, M. Zavertyaev^{10,b}, L. Zhang³, W.C. Zhang¹², Y. Zhang³, A. Zhelezov¹¹, A. Zhokhov³¹ and L. Zhong³.

¹ Centro Brasileiro de Pesquisas Físicas (CBPF), Rio de Janeiro, Brazil

² Universidade Federal do Rio de Janeiro (UFRJ), Rio de Janeiro, Brazil

³ Center for High Energy Physics, Tsinghua University, Beijing, China

⁴ LAPP, Université Savoie Mont-Blanc, CNRS/IN2P3, Annecy-Le-Vieux, France

⁵ Clermont Université, Université Blaise Pascal, CNRS/IN2P3, LPC, Clermont-Ferrand, France

⁶ CPPM, Aix-Marseille Université, CNRS/IN2P3, Marseille, France

⁷ LAL, Université Paris-Sud, CNRS/IN2P3, Orsay, France

⁸ LPNHE, Université Pierre et Marie Curie, Université Paris Diderot, CNRS/IN2P3, Paris, France

⁹ Fakultät Physik, Technische Universität Dortmund, Dortmund, Germany

¹⁰ Max-Planck-Institut für Kernphysik (MPIK), Heidelberg, Germany

¹¹ Physikalisches Institut, Ruprecht-Karls-Universität Heidelberg, Heidelberg, Germany

¹² School of Physics, University College Dublin, Dublin, Ireland

¹³ Sezione INFN di Bari, Bari, Italy

¹⁴ Sezione INFN di Bologna, Bologna, Italy

¹⁵ Sezione INFN di Cagliari, Cagliari, Italy

¹⁶ Sezione INFN di Ferrara, Ferrara, Italy

¹⁷ Sezione INFN di Firenze, Firenze, Italy

¹⁸ Laboratori Nazionali dell’INFN di Frascati, Frascati, Italy

¹⁹ Sezione INFN di Genova, Genova, Italy

²⁰ Sezione INFN di Milano Bicocca, Milano, Italy

²¹ Sezione INFN di Milano, Milano, Italy

²² Sezione INFN di Padova, Padova, Italy

²³ Sezione INFN di Pisa, Pisa, Italy

²⁴ Sezione INFN di Roma Tor Vergata, Roma, Italy

²⁵ Sezione INFN di Roma La Sapienza, Roma, Italy

²⁶ Henryk Niewodniczanski Institute of Nuclear Physics Polish Academy of Sciences, Kraków, Poland

- ²⁷ AGH - University of Science and Technology, Faculty of Physics and Applied Computer Science, Kraków, Poland
 - ²⁸ National Center for Nuclear Research (NCBJ), Warsaw, Poland
 - ²⁹ Horia Hulubei National Institute of Physics and Nuclear Engineering, Bucharest-Magurele, Romania
 - ³⁰ Petersburg Nuclear Physics Institute (PNPI), Gatchina, Russia
 - ³¹ Institute of Theoretical and Experimental Physics (ITEP), Moscow, Russia
 - ³² Institute of Nuclear Physics, Moscow State University (SINP MSU), Moscow, Russia
 - ³³ Institute for Nuclear Research of the Russian Academy of Sciences (INR RAN), Moscow, Russia
 - ³⁴ Budker Institute of Nuclear Physics (SB RAS) and Novosibirsk State University, Novosibirsk, Russia
 - ³⁵ Institute for High Energy Physics (IHEP), Protvino, Russia
 - ³⁶ Universitat de Barcelona, Barcelona, Spain
 - ³⁷ Universidad de Santiago de Compostela, Santiago de Compostela, Spain
 - ³⁸ European Organization for Nuclear Research (CERN), Geneva, Switzerland
 - ³⁹ Ecole Polytechnique Fédérale de Lausanne (EPFL), Lausanne, Switzerland
 - ⁴⁰ Physik-Institut, Universität Zürich, Zürich, Switzerland
 - ⁴¹ Nikhef National Institute for Subatomic Physics, Amsterdam, The Netherlands
 - ⁴² Nikhef National Institute for Subatomic Physics and VU University Amsterdam, Amsterdam, The Netherlands
 - ⁴³ NSC Kharkiv Institute of Physics and Technology (NSC KIPT), Kharkiv, Ukraine
 - ⁴⁴ Institute for Nuclear Research of the National Academy of Sciences (KINR), Kyiv, Ukraine
 - ⁴⁵ University of Birmingham, Birmingham, United Kingdom
 - ⁴⁶ H.H. Wills Physics Laboratory, University of Bristol, Bristol, United Kingdom
 - ⁴⁷ Cavendish Laboratory, University of Cambridge, Cambridge, United Kingdom
 - ⁴⁸ Department of Physics, University of Warwick, Coventry, United Kingdom
 - ⁴⁹ STFC Rutherford Appleton Laboratory, Didcot, United Kingdom
 - ⁵⁰ School of Physics and Astronomy, University of Edinburgh, Edinburgh, United Kingdom
 - ⁵¹ School of Physics and Astronomy, University of Glasgow, Glasgow, United Kingdom
 - ⁵² Oliver Lodge Laboratory, University of Liverpool, Liverpool, United Kingdom
 - ⁵³ Imperial College London, London, United Kingdom
 - ⁵⁴ School of Physics and Astronomy, University of Manchester, Manchester, United Kingdom
 - ⁵⁵ Department of Physics, University of Oxford, Oxford, United Kingdom
 - ⁵⁶ Massachusetts Institute of Technology, Cambridge, MA, United States
 - ⁵⁷ University of Cincinnati, Cincinnati, OH, United States
 - ⁵⁸ University of Maryland, College Park, MD, United States
 - ⁵⁹ Syracuse University, Syracuse, NY, United States
 - ⁶⁰ Pontifícia Universidade Católica do Rio de Janeiro (PUC-Rio), Rio de Janeiro, Brazil, associated to ²
 - ⁶¹ Institute of Particle Physics, Central China Normal University, Wuhan, Hubei, China, associated to ³
 - ⁶² Departamento de Física , Universidad Nacional de Colombia, Bogota, Colombia, associated to ⁸
 - ⁶³ Institut für Physik, Universität Rostock, Rostock, Germany, associated to ¹¹
 - ⁶⁴ National Research Centre Kurchatov Institute, Moscow, Russia, associated to ³¹
 - ⁶⁵ Yandex School of Data Analysis, Moscow, Russia, associated to ³¹
 - ⁶⁶ Instituto de Física Corpuscular (IFIC), Universitat de Valencia-CSIC, Valencia, Spain, associated to ³⁶
 - ⁶⁷ Van Swinderen Institute, University of Groningen, Groningen, The Netherlands, associated to ⁴¹
- ^a Universidade Federal do Triângulo Mineiro (UFTM), Uberaba-MG, Brazil
- ^b P.N. Lebedev Physical Institute, Russian Academy of Science (LPI RAS), Moscow, Russia
- ^c Università di Bari, Bari, Italy

- ^d *Università di Bologna, Bologna, Italy*
- ^e *Università di Cagliari, Cagliari, Italy*
- ^f *Università di Ferrara, Ferrara, Italy*
- ^g *Università di Firenze, Firenze, Italy*
- ^h *Università di Urbino, Urbino, Italy*
- ⁱ *Università di Modena e Reggio Emilia, Modena, Italy*
- ^j *Università di Genova, Genova, Italy*
- ^k *Università di Milano Bicocca, Milano, Italy*
- ^l *Università di Roma Tor Vergata, Roma, Italy*
- ^m *Università di Roma La Sapienza, Roma, Italy*
- ⁿ *Università della Basilicata, Potenza, Italy*
- ^o *AGH - University of Science and Technology, Faculty of Computer Science, Electronics and Telecommunications, Kraków, Poland*
- ^p *LIFAELS, La Salle, Universitat Ramon Llull, Barcelona, Spain*
- ^q *Hanoi University of Science, Hanoi, Viet Nam*
- ^r *Università di Padova, Padova, Italy*
- ^s *Università di Pisa, Pisa, Italy*
- ^t *Scuola Normale Superiore, Pisa, Italy*
- ^u *Università degli Studi di Milano, Milano, Italy*
- ^v *Politecnico di Milano, Milano, Italy*